Abstracta

Ano XXV - N. 01

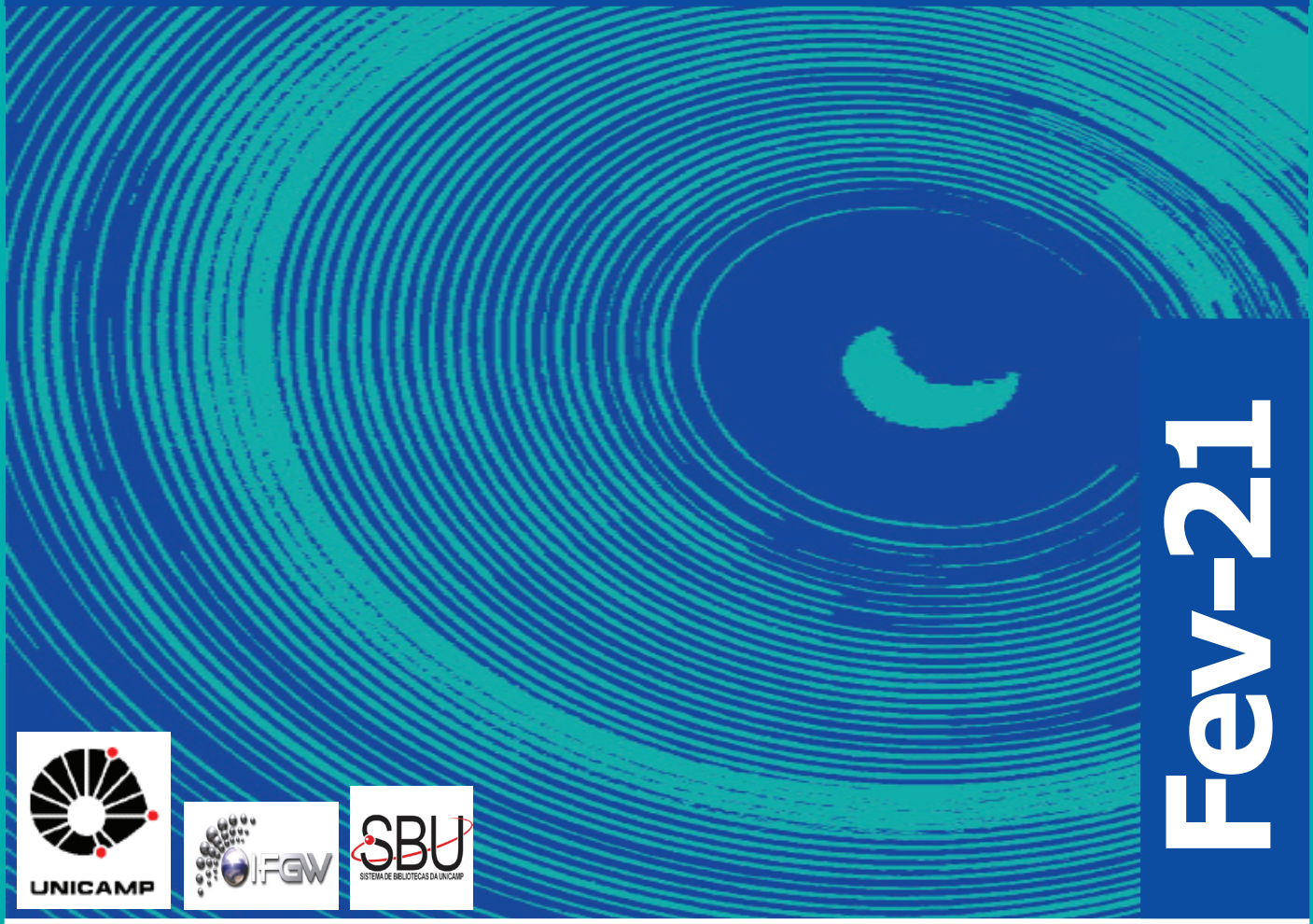

Fev-21

Artigos publicados 2020 - P367-2020 à P415-2020

Eventos publicados 2020 - P416-2020

Correções 2020 - Co003-2020

Artigos publicados 2021 - P001-2021 à P031-2021

Correções 2021 - Co001-2021 à Co002-2021

Material Editorial 2021 - Ma001-2021

Defesas de Dissertações do IFGW - D001-2020 à D002-2020

Defesas de Teses do IFGW - T001-2020

Artigos publicados 2020

[P367-2020] "A measurement of absolute efficiency of the ARAPUCA photon detector in liquid argon"

Totani, D.; Cancelo, G.; Cavanna, F.; **Escobar, C. O.*; Kemp, E.***; Marinho, F.; Paulucci, L.; Phan, D. D.; Mufson, S.; Macias, C.; Warner, D.

In the Fall of 2017, two photon detector designs for the Deep Underground Neutrino Experiment (DUNE) Far Detector were installed and tested in the TallBo liquid argon (LAr) cryostat at the Proton Assembly (PAB) facility, Fermilab. The designs include two light bars developed at Indiana University and a photon detector based on the ARAPUCA light trap engineered by Colorado State University and Fermilab. The performance of these devices is determined by analyzing 8 weeks of cosmic ray data. The current paper focuses solely on the ARAPUCA device as the performance of the light bars will be reported separately. The paper briefly describes the ARAPUCA concept, the TallBo setup, and focuses on data analysis and results.

JOURNAL OF INSTRUMENTATION 15[6], T06003, 2020. DOI: 10.1088/1748-0221/15/06/T06003

[P368-2020] "Alumina coating for dispersion management in ultra-high Q microresonators"

Inga, M.*; Fujii, L.*; Silva Filho, J. M. C. da*; Palhares, J. H. Q.; Ferlauto, A. S.; **Marques, F. C.*; Alegre, T. P. M.*; Wiederhecker, G.***

Silica optical microspheres often exhibit ultra-high quality factors, yet their group velocity dispersion, which is crucial for nonlinear optics applications, can only be coarsely tuned. We experimentally demonstrate that group-velocity dispersion of a silica microsphere can be engineered by coating it with conformal nanometric layers of alumina yet preserving its ultra-high optical quality factors (similar to 10(7)) at telecom wavelengths. Using the atomic layer deposition technique for the dielectric coating, which ensures nm-level thickness control, we not only achieve a fine dispersion tailoring but also maintain a low surface roughness and material absorption to ensure a low optical loss. Numerical simulations supporting our experimental results show that the alumina layer thickness is a promising technique for precise tuning of group-velocity dispersion. As an application, we demonstrate the generation of Kerr optical frequency combs, showing that the alumina coatings can also sustain the high optical intensities necessary for nonlinear optical phenomena.

APL PHOTONICS 5[11], 116107, 2020. DOI: 10.1063/5.0028839

[P369-2020] "Assumption-free measurement of the quantum state of light: Exploring the sidebands of intense fields"

Barbosa, F. A. S.*; Coelho, A. S.; Cassemiro, K. N.; Martinelli, M.; Nussenzveig, P.; Villar, A. S.

The quantum noise in photocurrent fluctuations usually gives incomplete information about the quantum state of spectral sideband modes of bright light beams involved in the detection. Each frequency component of the noise spectrum corresponds to two sideband modes symmetrically located around the bright optical field. In the case of the usual homodyne detection, it limits the ability to recover discriminated information of each mode involved. We theoretically show that complete reconstruction of the two-mode quantum state can be obtained by using phase-locked (coherent) resonator detection, even for non-Gaussian states. We experimentally demonstrate the technique by measuring a two-mode displaced coherent state.

PHYSICAL REVIEW A 102[6], 063705, 2020. DOI: 10.1103/PhysRevA.102.063705

[P370-2020] "Classical limits and contextuality in a scenario of multiple observers"

Baldijao, R. D.*; Cunha, M. T.

Contextuality is regarded as a nonclassical feature, challenging our everyday intuition; quantum contextuality is currently seen as a resource for many applications in quantum computation, being responsible for quantum advantage over classical analogs. In our work, we adapt the N-cycle scenarios with odd N to multiple independent observers which measure the system sequentially. We analyze the possibility of violating the inequalities as a function of the number of observers and under different measurement protocols. We then reinterpret the results as an open quantum system where the environment is divided into fragments. In this context, the results show the emergence of noncontextuality in such a setting, bringing together the quantum behavior to our classical experience. We then compare such emergence of noncontextuality with that of objectivity under the "environment as a witness" paradigm.

PHYSICAL REVIEW A 102[5], 052226, 2020. DOI: 10.1103/PhysRevA.102.052226

[P371-2020] "Consistent QFT description of non-standard neutrino interactions"

Falkowski, A.; Gonzalez-Alonso, M.; **Tabrizi, Z.***

Neutrino oscillations are precision probes of new physics. Apart from neutrino masses and mixings, they are also sensitive to possible deviations of low-energy interactions between quarks and leptons from the Standard Model predictions. In this paper we develop a systematic description of such non-standard interactions (NSI) in oscillation experiments within the quantum field theory framework. We calculate the event rate and oscillation probability in the presence of general NSI, starting from the effective field theory (EFT) in which new physics modifies the flavor or Lorentz structure of charged-current interactions between leptons and quarks. We also provide the matching between the EFT Wilson coefficients and the widely used simplified quantum-mechanical approach, where new physics is encoded in a set of production and detection NSI parameters. Finally, we discuss the consistency conditions for the standard NSI approach to correctly reproduce the quantum field theory result.

JOURNAL OF HIGH ENERGY PHYSICS 11, 48, 2020. DOI: 10.1007/JHEP11(2020)048

[P372-2020] "Crystallization, microstructure and polymorphic properties of soybean oil organogels in a hybrid structuring system"

Godoi, K. R. R de; Basso, R. C.; Ming, C. C.; Silva, A. A. da; **Cardoso, L. P.***; Ribeiro, A. P. B.

Organogels are semi-solid systems where the liquid phase is immobilized for three-dimensional network self-sustained formed by structuring agents capable to hold a larger quantity of liquid oil. The use of these structuring agents or crystallization modifiers, as specific triacylglycerols, emulsifiers and high molecular weight - high melting point lipids, have been recognized as the main alternative for obtaining low saturated fats for food formulation.

The aim of this work was to evaluate the crystallization, microstructure and polymorphism properties of hybrid soybean oil (SO) organogels, formulated with 6% (w:w) of structuring agents through a centroid simplex system added singly, in binary or ternary association of candelilla wax (CW), sorbitan monostearate (SMS) and fully hydrogenated palm oil (FHPO). The thermal behavior, crystallization kinetics, physical stability by temperature cyclization, microstructure and polymorphism were evaluated. FHPO and CW increased the stability and ability to form crystalline networks in organogels, while SMS accelerated the crystallization process. The structuring agents increased the initial and final crystallization temperatures, even as the melting temperatures and the enthalpy values of organogels. Time-temperature cyclization (cyclization 1: 5 degrees C/48 h + 35 degrees C/24 h + 5 degrees C/24 h; cyclization 2: 35 degrees C/48 h + 5 degrees C/72 h) showed that all the systems resulted in firm and stable organogels, except when SMS or FHPO were used singly. CW promoted formation of denser crystalline networks with higher solids content, quick crystallization onset and higher melting points that indicates adequate thermal resistance; while FHPO increased the solid content although it was effective to obtain organogels only at the cooling temperature (5 degrees C). The binary interaction of FHPO + CW increased the thermal resistance of organogels; and the interactions among SMS + CW and SMS + CW + FHPO although it was effective to obtain organogels. Regardless of the presence and proportions of structuring agents, organogels were characterized by beta polymorphism.

FOOD RESEARCH INTERNATIONAL 137, 109460, 2020. DOI: 10.1016/j.foodres.2020.109460

[P373-2020] "Dependence of inclusive jet production on the anti-k(T) distance parameter in pp collisions at root s=13 TeV"

Sirunyan, A. M.; Tumasyan, A.; Adam, W.; **Chinellato, J. A.*; Tonelli Manganote, E. J.***; et. al.; CMS Collaboration

The dependence of inclusive jet production in proton-proton collisions with a center-of-mass energy of 13 TeV on the distance parameter R of the anti-k(T) algorithm is studied using data corresponding to integrated luminosities up to 35.9 fb(-1) collected by the CMS experiment in 2016. The ratios of the inclusive cross sections as functions of transverse momentum p(T) and rapidity y, for R in the range 0.1 to 1.2 to those using R = 0.4 are presented in the region 84 < p(T)< 1588 GeV and |y|< 2.0. The results are compared to calculations at leading and next-to-leading order in the strong coupling constant using different parton shower models. The variation of the ratio of cross sections with R is well described by calculations including a parton shower model, but not by a leading-order quantum chromodynamics calculation including nonperturbative effects. The agreement between the data and the theoretical predictions for the ratios of cross sections is significantly improved when next-to-leading order calculations with nonperturbative effects are used.

JOURNAL OF HIGH ENERGY PHYSICS 12, 082, 2020. DOI: 10.1007/JHEP12(2020)082

[P374-2020] "Design of Compact Arbitrary-Ratio Multimode Power Splitters Based on Topological Derivative"

Ruiz, J. L. P.; Aldaya, I.; **Dainese, P.***; Gabrielli, L. H.

Compact unbalanced splitters are a key constitutive block to achieve flexibility in future multimode applications relying on silicon-on-insulator technology. Their design, however, poses significant challenges as it has to combine high performance for the different supported modes, a compact size, and compliance with fabrication constraints. In this letter, we employ topological derivative to optimize the design of bimodal unbalanced splitters with predefined split ratios of 2:1 and 3:1. Numerical simulations reveal that the optimized devices achieve the desired ratios with insertion losses of 0.6 dB and 0.5 dB, and crosstalks of -18.2 dB and -16.4 dB, both in a compact footprint of 4.2 mu m x 3.5 mu m.

IEEE PHOTONICS TECHNOLOGY LETTERS 32[18], 1187-1190, 2020. DOI: 10.1109/LPT.2020.3016012

[P375-2020] "Development of Nb2O5-doped ZnO/Carbon xerogel photocatalyst for the photodegradation of 4-chlorophenol"

Moraes, N. P. de; Santos, G. S. dos; Neves, G. C.; Valim, R. B.; Rocha, R. da S.; **Landers, R.***; Silva, M. L. C. P. da; Rodrigues, L. A.

This work evaluates the properties of a new Nb2O5-doped ZnO/carbon xerogel photocatalyst and its efficiency for the degradation of 4-chlorophenol under solar radiation. The development of this material is aimed at diminishing charge recombination during the photocatalytic process. The diffractograms obtained confirm the presence of the hexagonal zinc oxide structure in all samples, whereas the X-ray photoelectron spectroscopy confirms the presence of Nb2O5 on the structure of the ternary photocatalyst. The higher specific surface area of the Nb2O5-doped material, as well as the lower value of gap energy, can be ascribed to the presence of the newly incorporated metallic oxide into the structure of the materials, along with the carbon xerogel. The photocatalytic tests results show that the material with Nb2O5 in its composition exhibited superior efficiency in the degradation of 4-chlorophenol under simulated solar radiation, obtaining a much higher apparent reaction rate constant. Furthermore, the modification impacts the photocatalytic mechanism, which becomes greatly dependent on the hydroxyl radical.

OPTIK 219, 165238, 2020. DOI: 10.1016/j.ijleo.2020.165238

[P376-2020] "Dielectron production in proton-proton and proton-lead collisions at root s(NN)=5.02 TeV"

Acharya, S.; Adamova, D.; Adler, A.; **Albuquerque, D. S. D.*; Chinellato, D. D.*; Takahashi, J.***; et. all.; ALICE Collaboration

The first measurements of dielectron production at midrapidity (vertical bar eta(e)vertical bar < 0.8) in proton-proton and proton-lead collisions at root s(NN) = 5.02 TeV at the LHC are presented. The dielectron cross section is measured with the ALICE detector as a function of the invariant mass m(ee) and the pair transverse momentum p(T,ee) in the ranges m(ee) < 3.5 GeV/c(2) and p(T,ee) < 8 GeV/c, in both collision systems. In proton-proton collisions, the charm and beauty cross sections are determined at midrapidity from a fit to the data with two different event generators. This complements the existing dielectron measurements performed at root s = 7 and 13 TeV. The slope of the root s dependence of the three measurements is described by FONLL calculations. The dielectron cross section measured in proton-lead collisions is in agreement, within the current precision, with the expected dielectron production without any nuclear matter effects for e(+)e(-) pairs from open heavy-flavor hadron decays. For the first time at LHC energies, the dielectron production in proton-lead and proton-proton collisions are directly compared at the same root s(NN) via the dielectron nuclear modification factor R-pPb. The measurements are compared to model calculations including cold nuclear matter effects, or additional sources of dielectrons from thermal radiation.

PHYSICAL REVIEW C 102[5], 055204, 2020. DOI: 10.1103/PhysRevC.102.055204

[P377-2020] "Diverse interactions and ecosystem engineering can stabilize community assembly"

Yeakel, J. D.; **Pires, M. M.*; Aguiar, M. A. M. de***; O'Donnell, J. L.; Guimaraes, P. R.; Gravel, D.; Gross, T.

The complexity of an ecological community can be distilled into a network, where diverse interactions connect species in a web of dependencies. Species interact directly with each other and indirectly through environmental effects, however to our knowledge the role of these ecosystem engineers has not been considered in ecological network models. Here we explore the dynamics of ecosystem assembly, where species colonization and extinction depends on the constraints imposed by trophic, service, and engineering dependencies. We show that our assembly model reproduces many key features of ecological systems, such as the role of generalists during assembly, realistic maximum trophic levels, and increased nestedness with mutualistic interactions. We find that ecosystem engineering has large and nonlinear effects on extinction rates. While small numbers of engineers reduce stability by increasing primary extinctions, larger numbers of engineers increase stability by reducing primary extinctions and extinction cascade magnitude. Our results suggest that ecological engineers may enhance community diversity while increasing persistence by facilitating colonization and limiting competitive exclusion. The dynamics of ecological communities depends on interactions between species as well as those between species and their environment, however the effects of the latter are poorly understood. Here, Yeakel et al. reveal how species that modify their environment (ecosystem engineers) impact community dynamics and the risk of extinction.

NATURE COMMUNICATIONS 11[1], 2020. DOI: 10.1038/s41467-020-17164-x

[P378-2020] "Elliptic and triangular flow of (anti)deuterons in Pb-Pb collisions root S-NN=5.02 TeV"

Acharya, S.; Adamova, D.; Adler, A.; **Albuquerque, D. S. D.*; Chinellato, D. D.*; Takahashi, J.***; et. al.; ALICE Collaboration

The measurements of the (anti)deuteron elliptic flow (v(2)) and the first measurements of triangular flow (v(3)) in Pb-Pb collisions at a center-of-mass energy per nucleon-nucleon collision root S-NN = 5.02 TeV are presented. A mass ordering at low transverse momentum (p(T)) is observed when comparing these measurements with those of other identified hadrons, as expected from relativistic hydrodynamics. The measured (anti)deuteron v(2) lies between the predictions from the simple coalescence and blast-wave models, which provide a good description of the data only for more peripheral and for more central collisions, respectively. The mass number scaling, which is violated for v(2), is approximately valid for the (anti)deuterons v(3). The measured v(2) and v(3) are also compared with the predictions from a coalescence approach with phase-space distributions of nucleons generated by IEBE-VISHNU with AMPT initial conditions coupled with URQMD, and from a dynamical model based on relativistic hydrodynamics coupled to the hadronic afterburner SMASH. The model predictions are consistent with the data within the uncertainties in midcentral collisions, while a deviation is observed in the most central collisions.

PHYSICAL REVIEW C 102[5], 055203, 2020. DOI: 10.1103/PhysRevC.102.055203

[P379-2020] "Evidence for Top Quark Production in Nucleus-Nucleus Collisions"

Sirunyan, A. M.; Tumasyan, A.; Adam, W.; **Chinellato, J. A.*; Tonelli Manganote, E. J.***; et. all.; CMS Collaboration

Ultrarelativistic heavy ion collisions recreate in the laboratory the thermodynamical conditions prevailing in the early universe up to 10(-6) sec, thereby allowing the study of the quark--gluon plasma (QGP), a state of quantum chromodynamics (QCD) matter with deconfined partons. The top quark, the heaviest elementary particle known, is accessible in nucleus-nucleus collisions at the CERN LHC, and constitutes a novel probe of the QGP. Here, we report the first evidence for the production of top quarks in nucleus-nucleus collisions, using lead-lead collision data at a nucleon-nucleon center-of-mass energy of 5.02 TeV recorded by the CMS experiment. Two methods are used to measure the cross section for top quark pair production (sigma(t (t) over bar)) via the selection of charged leptons (electrons or muons) and bottom quarks. One method relies on the leptonic information alone, and the second one exploits, in addition, the presence of bottom quarks. The measured cross sections, sigma(t (t) over bar) = 2.54(-0.74)(+0.84) and 2.03(-0.64)(+0.71) mu b, respectively, are compatible with expectations from scaled proton-proton data and QCD predictions.

PHYSICAL REVIEW LETTERS 125[22], 222001, 2020. DOI: 10.1103/PhysRevLett.125.222001

[P380-2020] "First results on ProtoDUNE-SP liquid argon time projection chamber performance from a beam test at the CERN Neutrino Platform"

Abi, B.; Abud, A. Abed; Acciarri, R.; **Holanda, P. C. de*; Gelli, B.*; Guzzo, M. M.*; Kemp, E.*; Machado, A. A.*; Peres, O. L. G.*; Prakash, S.*; Reggiani-Guzzo, M.*; Segreto, E.*; Nunes, M. Soares*; Forero, D. Vanegas*; de Souza, H. Vieira***; et. al.

The ProtoDUNE-SP detector is a single-phase liquid argon time projection chamber with an active volume of 7.2 x 6.1 x 7.0 m(3). It is installed at the CERN Neutrino Platform in a specially-constructed beam that delivers charged pions, kaons, protons, muons and electrons with momenta in the range 0.3 GeV/c to 7 GeV/c. Beam line instrumentation provides accurate momentum measurements and particle identification. The ProtoDUNE-SP detector is a prototype for the first far detector module of the Deep Underground Neutrino Experiment, and it incorporates full-size components as designed for that module. This paper describes the beam line, the time projection chamber, the photon detectors, the cosmic-ray tagger, the signal processing and particle reconstruction. It presents the first results on ProtoDUNE-SP's performance, including noise and gain measurements, dE/dx calibration for muons, protons, pions and electrons, drift electron lifetime measurements, and photon detector noise, signal sensitivity and time resolution measurements. The measured values meet or exceed the specifications for the DUNE far detector, in several cases by large margins. ProtoDUNE-SP's successful operation starting in 2018 and its production of large samples of high-quality data demonstrate the effectiveness of the single-phase far detector design.

JOURNAL OF INSTRUMENTATION 15[12], P12004, 2020. DOI: 10.1088/1748-0221/15/12/P12004

[P381-2020] "Flexible Carbon Electrodes for Electrochemical Detection of Bisphenol-A, Hydroquinone and Catechol in Water Samples"

Sa, A. C. de; Barbosa, S. C.; .Pereira, P. A. R.; Wilson, D.; **Shimizu, F. M.***; Raposo, M.; Oliveira Jr., O. N.

The detection of pollutant traces in the public water supply and aquifers is essential for the safety of the population. In this article, we demonstrate that a simple electrochemical procedure in acidic solution can be employed for enhancing the sensitivity of flexible screen-printed carbon electrodes (SPEs) to detect bisphenol-A (BPA), hydroquinone, and catechol, simultaneously. The SPEs were pretreated electrochemically in a H2SO4 solution,

which did not affect their morphology, yielding high current signals with well separated oxidation peaks. The sensitivity values were 0.28, 0.230, and 0.056 mu A L mu mol(-1) with detection limits of 0.12, 0.82, and 0.95 mu mol L-1 for hydroquinone, catechol, and BPA, respectively. The sensors were reproducible and selective for detecting BPA in plastic cups, and with adequate specificity not to be affected by interferents from water samples. The simple, inexpensive, and flexible SPE may thus be used to detect emerging pollutants and monitor the water quality.

CHEMOSENSORS 8[4], 103, 2020. DOI: 10.3390/chemosensors8040103

[P382-2020] "Fragility of the Kondo insulating gap against disorder: Relevance to recent puzzles in topological Kondo insulators"

Sen, S.; Vidhyadhiraja, N. S.; **Miranda, E.*;** Dobrosavljevic, V.; Ku, W.

Kondo insulators are strongly correlated systems in which a clean insulating gap emerges only at very low temperature due to many-body effects involving localized f electrons. However, certain Kondo insulators, like SmB6 and Ce3Bi4Pt3, display metallic behaviors at extremely low temperature and have defied current understanding. Recent advances in topological effects in materials have raised attention on the protected surface states in these "topological Kondo insulators" as a potential resolution to some of the puzzling behaviors. Here we resolve these puzzles via a different route, by showing that the emergent Kondo insulating scale is extremely vulnerable against a moderate degree of disorder, such that the gap is filled with a small number of states. Therefore, the real samples are probably never truly insulating and this in turn compromises the essential building block of topological considerations. Our results suggest strongly that systems like the Slater insulators would be a more promising direction to extend the realm of topology to strongly correlated systems.

PHYSICAL REVIEW RESEARCH 2[3], 033370, 2020. DOI: 10.1103/PhysRevResearch.2.033370

[P383-2020] "Front-end control system and precise threshold configuration of the nu-Angra experiment"

Migliorini, M. L.; Fernandes, A., Jr.; Anjos, J. C.; Chimenti, P.; Costa, C. I. A.; **Gonzalez, L. F. G.***; Guedes, G. P.; **Kemp, E.***; Lima, H. P., Jr.; Lopes, G. S. P.; Lopes, A. S., Jr.; Nobrega, R. A.; Pains, I. F.; Pepe, I. M.; Ribeiro, D. B. S.; Souza, D. M.

The nu-Angra experiment aims to estimate the flux of antineutrino particles coming out from the Angra II nuclear reactor. Such flux is proportional to the thermal power released in the fission process and therefore can be used to infer the quantity of fuel that has been burned during a certain period. To do so, the nu-Angra Collaboration has developed an antineutrino detector and a complete acquisition system to readout and store the signals generated by its sensors. The entire detection system has been installed inside a container laboratory placed beside the dome of the nuclear reactor, in a restricted zone of the Angra II site. The system is supposed to work standalone for a few years in order to collect enough data so that the experiment can be validated. The detector's readout electronics and its environmental conditions are crucial parts of the experiment and they should work autonomously and be controlled and monitored remotely. Additionally, threshold configuration is a central issue of the experiment since antineutrino particles produce low energy signals in the detector, being necessary to carefully adjust it for all the detector channels in order to make the system capable of detecting signals as low as those generated by single photons. To this end, an embedded system was developed and integrated to the detection apparatus installed in the container at the Angra II site and is now operational and accessible to the nu-Angra Collaboration. This article aims at describing the proposed embedded system and presenting the results obtained during its commissioning phase.

JOURNAL OF INSTRUMENTATION 15[9], T09001, 2020. DOI: 10.1088/1748-0221/15/09/T09001

[P384-2020] "Inclusive search for highly boosted Higgs bosons decaying to bottom quark-antiquark pairs in proton--proton collisions at root s=13 TeV"

Sirunyan, A. M.; Tumasyan, A.; Adam, W.; **Chinellato, J. A.*; Tonelli Manganote, E. J.***; et. al.; CMS Collaboration

A search for standard model Higgs bosons (H) produced with transverse momentum (pT) greater than 450 GeV and decaying to bottom quark-antiquark pairs (bb¯¯¯¯) is performed using proton-proton collision data collected by the CMS experiment at the LHC at s√ = 13 TeV. The data sample corresponds to an integrated luminosity of 137 fb−1. The search is inclusive in the Higgs boson production mode. Highly Lorentz-boosted Higgs bosons decaying to bb¯¯¯¯ are reconstructed as single large-radius jets, and are identified using jet substructure and a dedicated b tagging technique based on a deep neural network. The method is validated with Z -- bb¯¯¯¯ decays. For a Higgs boson mass of 125 GeV, an excess of events above the background assuming no Higgs boson production is observed with a local significance of 2.5 standard deviations (σ), while the expectation is 0.7. The corresponding signal strength and local significance with respect to the standard model expectation are μH = 3.7 ± 1.2(stat)+0.8−0.7(syst)+0.8−0.5(theo) and 1.9 σ. Additionally, an unfolded differential cross section as a function of Higgs boson pT for the gluon fusion production mode is presented, assuming the other production modes occur at the expected rates.

JOURNAL OF HIGH ENERGY PHYSICS 12, 85, 2020. DOI: 10.1007/JHEP12(2020)085

[P385-2020] "Inducing micromechanical motion by optical excitation of a single quantum dot"

Kettler, J.; Vaish, N.; Lepinay, L. M. de; Besga, B.; **Assis, P. L. de***; Bourgeois, O.; Auffeves, A.; Richard, M.; Claudon, J.; Gerard, J. M.; Pigeau, B.; Arcizet, O.; Verlot, P.; Poizat, J. F.

Hybrid quantum optomechanical systems interface a single two-level system with a macroscopic mechanical degree of freedom. In a microwire with a single embedded semiconductor quantum dot, not only can the wire vibration modulate the excitonic transition energy, but the optical drive of the quantum dot can also induce motion in the wire. Hybrid quantum optomechanical systems(1) interface a macroscopic mechanical degree of freedom with a single two-level system such as a single spin(2-4), a superconducting qubit(5-7) or a single optical emitter(8-12). Recently, hybrid systems operating in the microwave domain have witnessed impressive progress(13,14). Concurrently, only a few experimental approaches have successfully addressed hybrid systems in the optical domain, demonstrating that macroscopic motion can modulate the two-level system transition energy(9,10,15). However, the reciprocal effect, corresponding to the backaction of a single quantum system on a macroscopic mechanical resonator, has remained elusive. In contrast to an optical cavity, a two-level system operates with no more than a single energy quantum. Hence, it requires a much stronger hybrid coupling rate compared to cavity optomechanical systems(1,16). Here, we build on the large strain coupling between an oscillating microwire and a single embedded quantum dot(9).

We resonantly drive the quantum dot's exciton using a laser modulated at the mechanical frequency. State-dependent strain then results in a time-dependent mechanical force that actuates microwire motion. This force is almost three orders of magnitude larger than the radiation pressure produced by the photon flux interacting with the quantum dot. In principle, the state-dependent force could constitute a strategy to coherently encode the quantum dot quantum state onto a mechanical degree of freedom(1).

NATURE NANOTECHNOLOGY 2020. DOI: 10.1038/s41565-020-00814-y

[P386-2020] "Insights into solid-state properties of dopamine and L-Dopa hydrochloride crystals through DFT calculations"

Araujo, R. L.; Lima Neto, J. X.; Henriques, J. M.; **Tromer, R. M.***; Barboza, C. A.; Oliveira, J. I. N.; Fulco, U. L.

We performed first-principle calculations based on density functional theory to investigate structural, electronic, optical, vibrational, and thermodynamic properties of the dopamine hydrochloride and Levodopa hydrochloride crystals. Our results showed a good agreement between the optimized structures and those determined previously by X-ray diffraction. The theoretical band gap of dopamine hydrochloride crystal was found to be indirect, whereas Levodopa hydrochloride showed a direct band gap. The calculated optical absorption of both crystalline structures occurs in the UV region, showing greater sensitivity to electromagnetic radiation with an energy of approximately 6 eV, and dielectric constant equal to 2.13 (2.15) for dopamine (Levodopa).

CHEMICAL PHYSICS LETTERS 761, 138033, 2020. DOI: 10.1016/j.cplett.2020.138033

[P387-2020] "Measurement of single-diffractive dijet production in proton-proton collisions at root s=8 TeV with the CMS and TOTEM experiments"

Sirunyan, A. M.; Tumasyan, A.; Adam, W.; **Chinellato, J. A.*; Tonelli Manganote, E. J.***; et. al.; CMS Collaboration; TOTEM Collaboration

Measurements are presented of the single-diffractive dijet cross section and the diffractive cross section as a function of the proton fractional momentum loss xi and the four-momentum transfer squared t. Both processes pp -> pX and pp -> Xp, i.e. with the proton scattering to either side of the interaction point, are measured, where X includes at least two jets; the results of the two processes are averaged. The analyses are based on data collected simultaneously with the CMS and TOTEM detectors at the LHC in proton-proton collisions at root s = 8 TeV during a dedicated run with beta* = 90 m at low instantaneous luminosity and correspond to an integrated luminosity of 37.5 nb(-1). The single-diffractive dijet cross section sigma(pX)(jj), in the kinematic region xi < 0.1, with at least two jets with transverse momentum p(T) > 40GeV, and pseudorapidity vertical bar eta vertical bar < 4.4, is 21.7 +/- 0.9(stat)(-3.3)(+3.0)(syst) +/- 0.9(lumi)nb. The ratio of the single-diffractive to inclusive dijet yields, normalised per unit of xi, is presented as a function of x, the longitudinal momentum fraction of the proton carried by the struck parton. The ratio in the kinematic region defined above, for x values in the range -2.9 <= log(10) x <= -1.6, is R = (sigma(pX)(jj)/Delta xi)/sigma(jj) = 0.025 +/- 0.001(stat) +/- 0.003(syst), where sigma(pX)(jj) and sigma(jj) are the single-diffractive and inclusive dijet cross sections, respectively. The results are compared with predictions from models of diffractive and nondiffractive interactions. Monte Carlo predictions based on the HERA diffractive parton distribution functions agree well with the data when corrected for the effect of soft rescattering between the spectator partons.

EUROPEAN PHYSICAL JOURNAL C 80[12], 1164, 2020. DOI: 10.1140/epjc/s10052-020-08562-y

[P388-2020] "Measurement of the top quark Yukawa coupling from t(t)over-bar kinematic distributions in the dilepton final state in proton-proton collisions at root s=13 TeV"

Sirunyan, A. M.; Tumasyan, A.; Adam, W.; **Chinellato, J. A.*; Tonelli Manganote, E. J.***; et. al.; CMS Collaboration

A measurement of the Higgs boson Yukawa coupling to the top quark is presented using proton-proton collision data at root s = 13 TeV, corresponding to an integrated luminosity of 137 fb(-1), recorded with the CMS detector. The coupling strength with respect to the standard model value, Y-t, is determined from kinematic distributions in t (t) over bar final states containing ee, mu mu, or e mu pairs. Variations of the Yukawa coupling strength lead to modified distributions for t (t) over bar production. In particular, the distributions of the t (t) over bar mass of the a system and the rapidity difference of the top quark and antiquark are sensitive to the value of Y-t. The measurement yields a best fit value of Y-t = 1.16(-0.35)(+0.24), bounding Y-t < 1.54 at a 95% confidence level.

PHYSICAL REVIEW D 102[9], 092013, 2020. DOI: 10.1103/PhysRevD.102.092013

[P389-2020] "Measurements of the W boson rapidity, helicity, double-differential cross sections, and charge asymmetry in pp collisions at root s=13 TeV"

Sirunyan, A. M.; Tumasyan, A.; Adam, W.; **Chinellato, J. A.*; Tonelli Manganote, E. J.***; et. al.; CMS Collaboration

The differential cross section and charge asymmetry for inclusive W boson production at root s = 13 TeV is measured for the two transverse polarization states as a function of the W boson absolute rapidity. The measurement uses events in which a W boson decays to a neutrino and either a muon or an electron. The data sample of proton-proton collisions recorded with the CMS detector at the LHC in 2016 corresponds to an integrated luminosity of 35.9 fb(-1). The differential cross section and its value normalized to the total inclusive W boson production cross section are measured over the rapidity range vertical bar y(w) vertical bar < 2.5. In addition to the total fiducial cross section, the W boson double-differential cross section, d(2)sigma/dp(T)(l)d vertical bar eta(l)vertical bar, and the charge asymmetry are measured as functions of the charged lepton transverse momentum and pseudorapidity. The precision of these measurements is used to constrain the parton distribution functions of the proton using the next-to-leading order NNPDF3.0 set.

PHYSICAL REVIEW D 102[9], 092012, 2020. DOI: 10.1103/PhysRevD.102.092012

[P390-2020] "Metallic islands in the Kondo insulator SmB6"

Souza, J. C.*; Rosa, P. F. S.; Sichelschmidt, J.; Carlone, M.; Venegas, P. A.; **Malcolms, M. O.*; Menegasso, P. M.*; Urbano, R. R.***; Fisk, Z.; **Pagliuso, P. G.***

The predicted interplay between Kondo physics and nontrivial topology in SmB6 has stimulated many experimental reports, some of which are in apparent contradiction.

The origin of the dispute may lie in the fragility of the Kondo insulating phase in the presence of Sm vacancies (Kondo holes) and/or natural impurities, such as Gd3+. In this work, we locally investigate this fragility for Al flux grown Sm1-xGdxB6 single crystals (0 <= x <= 0.02) by combining electron spin resonance (ESR) and complementary bulk measurements. The Gd3+ ESR spectra in a highly dilute regime (x similar to 0.0004) display the features of an insulating cubic environment. Remarkably, a metallic ESR line shape is observed for more concentrated samples (x similar to 0.004), even though these systems are still in a reasonably dilute regime and show insulating dc electrical resistivity. Our data indicate that the Kondo insulating state is destroyed locally around impurities before a global percolation occurs. This result not only explains the discrepancy between dc and ac conductivity but also provides a scenario to explain the presence of quantum oscillations in magnetization in the absence of quantum oscillations in electrical resistivity.

PHYSICAL REVIEW RESEARCH 2[4], 043181, 2020. DOI: 10.1103/PhysRevResearch.2.043181

[P391-2020] "Metastable solid 4He and the possible role of point defects"

Pedroso, V. Z.*; Zampronio, V.*; Vitiello, S. A.*

The metastable phase of solid 4He and the possible role of point defects in its destabilization are investigated by the introduction of a trial function of the shadow class with an explicit symmetrical kernel. This is a trial function that ensures the possible exchange of atoms and the delocalization of atoms and defects in a very effective manner. We show that the formation energy for vacancies is equal to zero at a pressure Pc = 20 ± 2 atm, which is in excellent agreement with the experimental observation. The pressure at which a self--interstitial also has a formation energy equal to zero, is in agreement with the density where vacancies have the same property. Formation energies of a 3He interstitial or a substitutional impurity were estimated. Other properties of interest for systems made from 4He atoms are estimated and compared with results from the literature whenever available.

Journal of Physics: Condensed Matter 33[7], 075901, 2020. DOI: 10.1088/1361-648X/abc5d6

[P392-2020] "Microdosimetric calculations for radionuclides emitting beta and alpha particles and Auger electrons"

Seniwal, B.; **Bernal, M. A.***; Fonseca, T. C. F.

This work focuses on the calculation of S-values and radial energy profiles for radionuclides emitting high (Y-90, Sr-89), medium (Re-186, Sm-153) and low-energy (Er-169, Lu-177) beta-particles, Auger electrons (In-111, Ga-67, I-123) and alpha-particles (At-211, Ac-225). Simulations were performed using the EGSnrc and GEANT4-DNA Monte Carlo (MC) codes for a spherical cell geometry. S-values were computed using decay spectra available in literature for Tc-99m and In-111. To investigate the effect on S-value when the same emission spectrum is used in two different MC codes. Internal modules of the MC codes were used to simulate the decay of other radionuclides mentioned above. Radial energy profiles for uniformly distributed radioactive sources in the cell nucleus and cytoplasm were calculated and results were compared with the literature. For S-values calculated using the same emission spectrum, the results showed good agreement with each other and with the literature. Whereas, the S-values calculated using the internal decay data of the MC codes, for instance, for Ga-67 and Y-90, showed discrepancies up to 40%. Radial energy profiles were also different from those reported in the literature. Our results show that well validated radiation emission spectra must be used for such calculations and internal decay spectra of MC codes should be used with caution. The normalized probability density functions must be used to sample points uniformly into spherical volumes and the methodology proposed here can be used to correctly determine radial energy profiles.

APPLIED RADIATION AND ISOTOPES 166, 109302, 2020. DOI: 10.1016/j.apradiso.2020.109302

[P393-2020] "Micromagnetic simulations of magnetization reversal in kagome artificial spin ice"

Velo, M. F.*; Cecchi, B. M.*; Pirota, K. R.*

This work reports micromagnetic simulations used to study magnetization reversal in kagome artificial spin ice, taking into account the actual edge imperfections presented by the magnetic nanoislands as a source of disorder. An important advantage of the micromagnetic approach is to discretize a magnetic element in nanometric domains, allowing access to the sample magnetic moments distribution in detail. The limit case of zero disorder is accessed considering a system composed of perfect magnetic islands. The main result is the prediction of a critical angle between the applied magnetic field and the direction of one of the sublattices, above which Dirac strings emerge. For lower values, the reversal occurs through a bidimensional fashion, being smooth or abrupt depending on whether or not roughness is present, respectively. Finally, our simulations open the question of how the contour imperfections really influence the magnetic response of artificial spin ice.

PHYSICAL REVIEW B 102[22], 224420, 2020. DOI: 10.1103/PhysRevB.102.224420

[P394-2020] "Model-Based Design and Simulation of Paraxial Ray Optics Systems"

Fujiwara, E.; **Cordeiro, C. M. B.***

A model-based design allows representing complex, multi-domain systems as interconnected functional blocks, yielding graphical, intuitive information about the overall project, besides simplifying simulation. This work proposes using the modular approach as an optical engineering design and educational tool for developing paraxial ray optics setups, providing further integration with mechatronics subsystems and control loops. An expanded version of the ABCD transfer matrix modeling is implemented in MATLAB Simulink environment to simultaneously perform ray tracing and dynamic simulations. The methodology is validated for different problems, including paraxial cloaking, transmission through a multimode optical fiber, a Fabry--Perot interferometer, and an optical pickup with automatic focus, yielding reliable results with prospective applications in optical engineering design and for creating virtual labs devoted to multiphysics and mechatronics engineering courses.

APPLIED SCIENCES-BASEL 10[22], 8278, 2020. DOI: 10.3390/app10228278

[P395-2020] "Multipolar effects in the hysteresis behavior of 2D arrays of compass needles: Experiments and simulations"

Velo, M. F.*; Cecchi, B. M.*; Béron, F.*; Pirota, K. R.*

Despite its easy experimental implementation, macroscopic systems composed of compass needles array show a rich and complex variety of physical phenomena that are not yet fully understood.

In this work we consider the experimental realization of a square lattice of equally spaced millimeter sized compass needles, as well as its theoretical approach taking into account a proper higher order moments expansion of the magnetic potential, considering the actual shape of a compass needle. A Monte Carlo simulation, done using interaction energy value given by the previous expansion, showed excelent agreement with experimental results for the squared array magnetization process. Rather than the unique commonly considered dipolar contribution, the results evidence the importance of multipole expansion in considering interactions among magnetic elements with finite size, attributing to the magnetic particle shape a critical importance that could raise higher order contributions. In addition to the clear pedagogical relevance, the conclusions deserve attention, and reopen the discussion of whether dipolar interaction is the only relevant contribution to be considered in theoretical models in which magnetostatic interactions are important, e.g. superparamagnetic nanoparticles models.

Physics Open 5, 100041, 2020. DOI: 10.1016/j.physo.2020.100041

[P396-2020] "Non-Newtonian flow effects in supercooled water"

Ribeiro, I. de A.; **Koning, M. de***

The viscosity of supercooled water has been a subject of intense study, in particular with respect to its temperature dependence. Much less is known, however, about the influence of dynamical effects on the viscosity in its supercooled state. Here we address this issue for the first time, using molecular dynamics simulations to investigate the shear-rate dependence of the viscosity of supercooled water as described by the TIP4P/Ice model. We show the existence of a distinct crossover from Newtonian to non-Newtonian behavior characterized by a power-law shear-thinning regime. The viscosity reduction is due to the decrease in the connectivity of the hydrogen-bond network. Moreover, the shear thinning intensifies as the degree of supercooling increases, whereas the crossover flow rate is approximately inversely proportional to the Newtonian viscosity. These results stimulate further investigation into possible fundamental relations between these nonequilibrium effects and the quasistatic Newtonian viscosity behavior of supercooled water.

PHYSICAL REVIEW RESEARCH 2[2], 022004, 2020. DOI: 10.1103/PhysRevResearch.2.022004

[P397-2020] "Observation of electroweak production of W gamma with two jets in proton-proton collisions at root s=13 TeV"

Sirunyan, A. M.; Tumasyan, A.; Adam, W.; **Chinellato, J. A.*; Tonelli Manganote, E. J.*;** et. all.; CMS Collaboration

A first observation is presented for the electroweak production of a W boson, a photon, and two jets in proton-proton collisions. The W boson decays are selected by requiring one identified electron or muon and an imbalance in transverse momentum. The two jets are required to have a high dijet mass and a large separation in pseudorapidity. The measurement is based on data collected with the CMS detector at a center-of--mass energy of 13 TeV, corresponding to an integrated luminosity of 35.9 fb(-1). The observed (expected) significance for this process is 4.9 (4.6) standard deviations. After combining with previously reported CMS results at 8 TeV, the observed (expected) significance is 5.3 (4.8) standard deviations. The cross section for the electroweak W gamma jj production in a restricted fiducial region is measured as 20.4 +/- 4.5 fb and the total cross section for W gamma production in association with 2 jets in the same fiducial region is 108 +/- 16 fb. All results are in good agreement with recent theoretical predictions. Constraints are placed on anomalous quartic gauge couplings in terms of dimension-8 effective field theory operators.

PHYSICS LETTERS B 811, 135988, 2020. DOI: 10.1016/j.physletb.2020.135988

[P398-2020] "Odd-frequency superconductivity in dilute magnetic superconductors"

Santos, F. L. N.; Perrin, V.; Jamet, F.; Civelli, M.; Simon, P.; Aguiar, M. C. O.; **Miranda, E.***; Rozenberg, M. J.

We show that dilute magnetic impurities in a conventional superconductor give origin to an odd-frequency component of superconductivity, manifesting itself in Yu-Shiba-Rusinov bands forming within the bulk superconducting gap. Our results are obtained in a general model solved within the dynamical mean field theory. By exploiting a disorder analysis and the limit to a single impurity, we are able to provide general expressions that can be used to extract explicitly the odd-frequency superconducting function from scanning tunneling measurements.

PHYSICAL REVIEW RESEARCH 2[3], 033229, 2020. DOI: 10.1103/PhysRevResearch.2.033229

[P399-2021] "O Radiômetro de Crookes é um cata-luz"

Lunazzi, J. J.*; Souza, A. M. de*

Dentre os experimentos mais importantes do século XIX está um que liga o eletromagnetismo com a mecânica de forma direta. No chamado "Radiômetro de Crookes" a luz, empurrando palhetas, surpreende dando a imediata percepção de sua energia. O público percebe que o lado preto é quem recebe a maior ação. O estudante de escola, e o universitário, tentam entender o porquê disso, mas ficam com dúvidas. Neste artigo fazemos um recenso das dúvidas que acontecem, em nível de escola, graduação, e pós-graduação. É comum pensar em termos de eletromagnetismo, de termodinâmica, mas não conhecemos artigo algum que tenha incluído o atrito na análise. Mostramos aqui a influência do atrito por meio de um experimento simples.

Revista Brasileira de Ensino de Física 43, e20200357, primeira data de publicação: NOV 2020. DOI: 10.1590/1806-9126-rbef-2020-0357

[P400-2020] "Performance of the CMS Level-1 trigger in proton-proton collisions at root s=13 TeV"

Sirunyan, A. M.; Tumasyan, A.; Adam, W.; **Chinellato, J. A.*; Manganote, E. J. T***; et al. CMS Collaboration

At the start of Run 2 in 2015, the LHC delivered proton-proton collisions at a center-ofmass energy of 13 TeV. During Run 2 (years 2015-2018) the LHC eventually reached a luminosity of 2.1 x 10(34) cm(-2) s(-1), almost three times that reached during Run 1 (2009-2013) and a factor of two larger than the LHC design value, leading to events with up to a mean of about 50 simultaneous inelastic proton-proton collisions per bunch crossing (pileup). The CMS Level-1 trigger was upgraded prior to 2016 to improve the selection of physics events in the challenging conditions posed by the second run of the LHC. This paper describes the performance of the CMS Level-1 trigger upgrade during the data taking period of 2016-2018. The upgraded trigger implements pattern recognition and boosted decision tree regression techniques for muon reconstruction, includes pileup subtraction for jets and energy sums, and incorporates pileup--dependent isolation requirements for electrons and tau leptons.

In addition, the new trigger calculates high-level quantities such as the invariant mass of pairs of reconstructed particles. The upgrade reduces the trigger rate from background processes and improves the trigger efficiency for a wide variety of physics signals.

JOURNAL OF INSTRUMENTATION 15[10], P10017, 2020. DOI: 10.1088/1748-0221/15/10/P10017

[P401-2020] "Polyfuran-based chemical sensors: Identification of promising derivatives via DFT calculations and fully atomistic reactive molecular dynamics"

Lascane, L. G.; **Oliveira, E. F.*; Galvão, D. S.***; Batagin Neto, A.

Organic polymers are promising materials for the design of active layers of chemical sensors. In this context, polyfuran (PF) derivatives have not been largely investigated, mainly due to stability problems and poorer electrical properties. Recent works have demonstrated that some of these typical drawbacks can be overcome by an appropriate choice of side groups, allowing the application of these compounds in varied areas, including in chemical sensors. To better evaluate the sensory features of these materials, electronic structure calculations (DFT) and fully atomistic reactive molecular dynamics (FARMD) simulations were conducted to investigate the local reactivity and analyze possible adsorption processes. The obtained results indicate the compounds PF-CCH and PF-NO2 as the most promising materials for the development of chemical sensors. These derivatives present high reactivity on the side groups, high stability to oxidation and good responses to the presence of analytes. Our results also indicate that the analysis of local reactivities via DFT (condensed-to-atoms Fukui indexes) and FARMD simulations can be used in a complementary way to evaluate polymer sensory properties and adsorption processes.

EUROPEAN POLYMER JOURNAL 141, 110085, 2020. DOI: 10.1016/j.eurpolymj.2020.110085

[P402-2020] "Probing the structure of the initial state of heavy-ion collisions with P-T-dependent flow fluctuations"

Hippert, M.*; Barbon, J. G. P.*; Chinellato, D. D.*; Luzum, M.; Noronha, J.; Nunes da Silva, T.; **Serenone, W. M.*; Takahashi, J.***; ExTrEMe Collaboration

The connection between initial-state geometry and anisotropic flow can be quantified through a well-established mapping between P-T-integrated flow harmonics and cumulants of the initial transverse energy distribution. In this paper we successfully extend this mapping to also include P-T-differential flow. In doing so, we find that subleading principal components of anisotropic flow can reveal previously unobserved details of the hydrodynamic response, in both the linear and the nonlinear regimes. Most importantly, we show that they provide novel information on the small-scale structures present in the initial stage of relativistic heavy-ion collisions.

PHYSICAL REVIEW C 102 [6], 064909, 2020. DOI: 10.1103/PhysRevC.102.064909

[P403-2020] "Production of omega mesons in pp collisions at s=7 TeV"

Acharya, S.; Adamova, D.; Adler, A.; **Albuquerque, D. S. D.*; Chinellato, D. D.*; Takahashi, J.***; et. all.; ALICE Collaboration

The invariant differential cross section of inclusive omega (782) meson production at midrapidity (|y|<0.5) in pp collisions at s=7 TeV was measured with the ALICE detector at the LHC over a transverse momentum range of 2<pT<17 GeV/c. The omega meson was reconstructed via its omega -> pi+pi-pi 0 decay channel. The measured omega production cross section is compared to various calculations: PYTHIA 8.2 Monash 2013 describes the data, while PYTHIA 8.2 Tune 4C overestimates the data by about 50%. A recent NLO calculation, which includes a model describing the fragmentation of the whole vector-meson nonet, describes the data within uncertainties below 6 GeV/c, while it overestimates the data by up to 50% for higher pT. The omega/pi 0 ratio is in agreement with previous measurements at lower collision energies and the PYTHIA calculations. In addition, the measurement is compatible with transverse mass scaling within the measured pT range and the ratio is constant with C omega/pi 0=0.67 +/- 0.03(stat) +/- 0.04(sys) above a transverse momentum of 2.5 GeV/c.

EUROPEAN PHYSICAL JOURNAL C 80 [12], 1130, 2020. DOI: 10.1140/epjc/s10052-020-08651-y

[P404-2020] "Quasinormal-Mode Perturbation Theory for Dissipative and Dispersive Optomechanics"

Primo, A. G.*; Carvalho, N. C.*; Kersul, C. M.*; Frateschi, N. C.*; Wiederhecker, G. S.*; Alegre, T. P. M.*

Despite the several novel features arising from the dissipative optomechanical coupling, such effect remains vastly unexplored due to the lack of a simple formalism that captures non-Hermiticity in the engineering of optomechanical systems. In this Letter, we show that quasinormal-mode-based perturbation theory is capable of correctly predicting both dispersive and dissipative optomechanical couplings. We validate our model through simulations and also by comparison with experimental results reported in the literature. Finally, we apply this formalism to plasmonic systems, used for molecular optomechanics, where strong dissipative coupling signatures in the amplification of vibrational modes could be observed.

PHYSICAL REVIEW LETTERS 125[23], 233601, 2020. DOI: 10.1103/PhysRevLett.125.233601

[P405-2020] "Real-Time Monitoring of Neurocritical Patients with Diffuse Optical Spectroscopies"

Forti, R. M.*; Katsurayama, M.; Valler, L.; **Quiroga, A.*; Simioni, L.***; Menko, J.; Falcao, A. L. E.; Li, L. M.; **Mesquita, R. C.***

Neurophysiological monitoring is an important goal in the treatment of neurocritical patients, as it may prevent secondary damage and directly impact morbidity and mortality rates. However, there is currently a lack of suitable non-invasive, real-time technologies for continuous monitoring of cerebral physiology at the bedside. Diffuse optical techniques have been proposed as a potential tool for bedside measurements of cerebral blood flow and cerebral oxygenation in case of neurocritical patients. Diffuse optical spectroscopies have been previously explored to monitor patients in several clinical scenarios ranging from neonatal monitoring to cerebrovascular interventions in adults. However, the feasibility of the technique to aid clinicians by providing real-time information at the bedside remains largely unaddressed. Here, we report the translation of a diffuse optical system for continuous real-time monitoring of cerebral blood flow, cerebral oxygenation, and cerebral oxygen metabolism during intensive care. The real-time feature of the instrument could enable treatment strategies based on patient-specific cerebral physiology rather than relying on surrogate metrics, such as arterial blood pressure.

By providing real-time information on the cerebral circulation at different time scales with relatively cheap and portable instrumentation, this approach may be especially useful in low-budget hospitals, in remote areas and for monitoring in open fields (e.g., defense and sports).

JOVE-JOURNAL OF VISUALIZED EXPERIMENTS 165, e61608, 2020. DOI: 10.3791/61608

[P406-2020] "Reconstruction of events recorded with the surface detector of the Pierre Auger Observatory"

Aab, A.; Abreu, P.; Aglietta, M.; **Chinellato, J. A.*; Franco, D. de O.*; Castro, M. L. D.*; Dobrigkeit, C.*; Fauth, A. C.*; Payeras, A. M.*; Muller, M. A.***; et al. Pierre Auger Collaboration

Cosmic rays arriving at Earth collide with the upper parts of the atmosphere, thereby inducing extensive air showers. When secondary particles from the cascade arrive at the ground, they are measured by surface detector arrays. We describe the methods applied to the measurements of the surface detector of the Pierre Auger Observatory to reconstruct events with zenith angles less than 60 degrees using the timing and signal information recorded using the water-Cherenkov detector stations. In addition, we assess the accuracy of these methods in reconstructing the arrival directions of the primary cosmic ray particles and the sizes of the induced showers.

JOURNAL OF INSTRUMENTATION 15[10], P10021, 2020. DOI: 10.1088/1748-0221/15/10/P10021

[P407-2020] "Search for bottom-type, vectorlike quark pair production in a fully hadronic final state in proton-proton collisions at root s=13 TeV"

Sirunyan, A. M.; Tumasyan, A.; Adam, W.; **Chinellato, J. A.*; Tonelli Manganote, E. J.***; et. al.; CMS Collaboration

A search is described for the production of a pair of bottom--type vectorlike quarks (VLQs), each decaying into a b or (b) over bar quark and either a Higgs or a Z boson, with a mass greater than 1000 GeV. The analysis is based on data from proton-proton collisions at a 13 TeV center-of-mass energy recorded at the CERN LHC, corresponding to a total integrated luminosity of 137 fb(-1). As the predominant decay modes of the Higgs and Z bosons are to a pair of quarks, the analysis focuses on final states consisting of jets resulting from the six quarks produced in the events. Since the two jets produced in the decay of a highly Lorentz-boosted Higgs or Z boson can merge to form a single jet, nine independent analyses are performed, categorized by the number of observed jets and the reconstructed event mode. No signal in excess of the expected background is observed. Lower limits are set on the VLQ mass at 95% confidence level equal to 1570 GeV in the case where the VLQ decays exclusively to a b quark and a Higgs boson, 1390 GeV for when it decays exclusively to a b quark and a Z boson, and 1450 GeV for when it decays equally in these two modes. These limits represent significant improvements over the previously published VLQ limits.

PHYSICAL REVIEW D 102[11], 112004, 2020. DOI: 10.1103/PhysRevD.102.112004

[P408-2020] "Search for decays of the 125 GeV Higgs boson into a Z boson and a rho or phi meson"

Sirunyan, A. M.; Tumasyan, A.; Adam, W.; **Chinellato, J. A.*; Tonelli Manganote, E. J.***; et. al.; CMS Collaboration

Decays of the 125 GeV Higgs boson into a Z boson and a rho (0)(770) or (1020) meson are searched for using proton-proton collision data collected by the CMS experiment at the LHC at <mml:msqrt>s</mml:msqrt> = 13 TeV. The analysed data set corresponds to an integrated luminosity of 137 fb(-1). Events are selected in which the Z boson decays into a pair of electrons or a pair of muons, and the rho and phi mesons decay into pairs of pions and kaons, respectively. No significant excess above the background model is observed. As different polarization states are possible for the decay products of the Z boson and rho or phi mesons, affecting the signal acceptance, scenarios in which the decays are longitudinally or transversely polarized are considered. Upper limits at the 95% confidence level on the Higgs boson branching fractions into Z rho and Z phi are determined to be 1.04-1.31% and 0.31-0.40%, respectively, where the ranges reflect the considered polarization scenarios; these values are 740-940 and 730-950 times larger than the respective standard model expectations. These results constitute the first experimental limits on the two decay channels.

JOURNAL OF HIGH ENERGY PHYSICS 11, 39, 2020. DOI: 10.1007/JHEP11(2020)039

[P409-2020] "Spin-orbit implementation of the Solovay-Kitaev decomposition of single-qubit channels"

Passos, M. H. M.; **Oliveira Junior, A. de*; Oliveira, M. C. de***; Khoury, A. Z.; Huguenin, J. A. O.

The Solovay-Kitaev theorem allows us to approximate any single-qubit gate to arbitrary accuracy with a finite sequence of fundamental operations from a universal set of gates. Inspired by this decomposition, we present a quantum channel simulator capable of implementing any completely positive trace-preserving map. Our realization consists of one ancillary qubit, encoded in the transverse mode of a laser beam (orbital degree of freedom), one qubit system, encoded in its polarization (spin), one spin-orbit CNOT gate, and four single-qubit operations performed with prisms and polarization components. Our results describe the implementation of arbitrary single-qubit channels on the photon polarization using the transverse mode as the ancillary qubit.

PHYSICAL REVIEW A 102[6], 062601, 2020. DOI: 10.1103/PhysRevA.102.062601

[P410-2020] "Splitting up entropy into vibrational and configurational contributions in bulk metallic glasses: A thermodynamic approach"

Donado, R. A.*; Antonelli, A.*

We apply an efficient methodology to separate vibrational and configurational entropies in bulk metallic glasses by means of molecular dynamics simulation based on a combination of nonequilibrium adiabatic switching and reversible scaling methods. This approach involves calculating the vibrational free energy using the Einstein crystal as a reference for the solid phase and the recently proposed Uhlenbeck-Ford model for the fluid phase. This methodology has the advantage that it does not require a crystalline solid phase for separating the entropies. Therefore, in principle, it is applicable to any material, regardless of whether or not it has a crystalline phase. Using this methodology, we separate the vibrational and configurational entropies of two metallic glasses with different fragilities at zero external pressure, namely, Cu50Zr50 and Cu46Zr46Al8. We find that the results for the former alloy are in quite reasonable agreement with recent experimental work by Smith et al. [Nat. Phys. 13, 900 (2017)]. We also find the configurational entropy of the glass containing Al to be 70% larger than that of the other glass.

Our results suggest that although other factors may be at play, the configurational entropy can be used to investigate the effect of the addition of a minor-alloying element on the glass-forming ability of bulk metallic glasses.

PHYSICAL REVIEW RESEARCH 2[1], 013202, 2020. DOI: 10.1103/PhysRevResearch.2.013202

[P411-2020] "The effects of limonene on the crystallization of palm oil"

Mello, N. A.; **Cardoso, L. P.***; Ribeiro, A. P. B.; Bicas, J. L.

This study aimed to evaluate how the addition of limonene in different concentrations (1-10 g/100 g) influences the crystallization of palm oil (PO). An extensive study of the crystallization behavior of PO and its blends was performed using nuclear magnetic resonance (NMR), differential scanning calorimetry (DSC), polarized light microscopy (PLM), and X-ray diffraction. Adding limonene to PO reduced its solid fat content (SFC) and delayed crystallization, with a more pronounced effect at higher concentrations (7.5 and 10 g/100 g). The samples' microstructure changed from spherulites in pure PO to agglomerated granular crystals at higher concentrations (7.5 and 10 g/100 g). Regarding polymorphism, the samples containing limonene showed a slight sign of acceleration over time, and after 60 days all samples, including PO, had predominance of the beta form. It can be affirmed that reducing the SFC of PO substantially contributes to mitigating its post-hardening.

LWT-FOOD SCIENCE AND TECHNOLOGY 133, 110079, 2020. DOI: 10.1016/j.lwt.2020.110079

[P412-2020] "The response of boronized 34CrAlMo5-10 (EN41B) steel to nanoindentation, oxidation, and wear"

Litoria, A. K.; Joshi, M. D.; **Antunes, V.***; Singh, D.; Figueroa, C. A.; **Alvarez, F.***; Hosmani, S. S.

The present study deals with the properties of boronized and non-boronized low-alloy steel (34CrAlMo5-10). Specimens are characterised using microscopy, various spectroscopic techniques, nanoindentation, surface profilometer, and tribometer. The boronized region contains (i) (Fe, M)(2)B columns and (ii) matrix between the columns. Nanoindentation study reveals the difference in the mechanical behaviour of boride, matrix, and core regions. Strain-rate sensitivity of different regions of the specimen cross-section varies between 0.005 and 0.011. The boride phase is more sensitive to the strain-rate than matrix and core. The room-temperature oxidation resistance of the steel surface is enhanced by the presence of a higher proportion of mixed-boride and the oxide layer enriched with Cr2O3. At 550 and 850 degrees C, boronized specimens have higher oxidation resistance than the non-boronized specimens, where the layer of iron-borates protects the surface. At 200 degrees C, the boronized specimen has deprived oxidation resistance. Amongst the investigated wear-parameters, the maximum and minimum wear-resistance of the boronized surface is about 46 and 8 times the wear-resistance of the non-boronized surface, respectively. A steeper drop in the tribological advantage gained by the boronizing treatment is perceived with the increase in load, especially under higher sliding speed.

PHILOSOPHICAL MAGAZINE, Primeira data de acesso: 30 de dezembro de 2020. DOI: 10.1080/14786435.2020.1866221

[P413-2020] "Time evolution of the quantized field coupled to a thermal bath: A phase space approach"

Mattos, E. P.*; Vidiella-Barranco, A.*

We present an alternative method for describing the evolution of a mode of the quantized electromagnetic field in contact with a finite temperature thermal bath. We employ the expansion of the field density operator in terms of coherent states and the related Glauber-Sudarshan P-function in phase space. The method allows us to obtain analytical expressions of the system's time-evolved P-function without needing to solve the corresponding master equation.

ANNALS OF PHYSICS 422, 168321, 2020. DOI: 10.1016/j.aop.2020.168321

[P414-2020] "Visible light-driven ZnO/g-C3N4/carbon xerogel ternary photocatalyst with enhanced activity for 4-chlorophenol degradation"

Sousa, J. G. M. de; Silva, T. V. C. da; Moraes, N. P. de; Silva, M. L. C. P. da; Rocha, R. da S.; **Landers, R.***; Rodrigues, L. A.

This work aims to synthesize visible light-driven photocatalysts based on zinc oxide, polymeric graphitic carbon nitride (g-C3N4) and carbon xerogel. The addition of g-C3N4 and carbon xerogel to the zinc oxide is expected to hinder electron-vacancy recombination, increase specific surface area and reduce bandgap energy. The Raman spectroscopy and X-ray diffractometry confirm the presence of the wurtzite phase of zinc oxide in the materials. Furthermore, the X-ray diffractometry results show that C and N were likely incorporated into the structure of the zinc oxide in the ternary and binary materials, due to the distortion observed in the crystal lattice of the composites. The XPS analysis corroborates the presence of the g-C3N4 in the composite developed, as well as the incorporation of the carbon xerogel into the wurtzite structure. The addition of g-C3N4 and carbon xerogel resulted in significant changes on the morphology of the prepared materials, causing an increase in surface area and textural modification. The optimized ternary composite, which contains 0.25% of g-C3N4 (% w/w), has the highest photocatalytic response among all materials tested, obtaining 92% of 4-chlorophenol degradation under solar radiation and 72% under visible radiation, after 5 h. The enhanced photocatalytic activity of the ternary material can be linked to a superior charge mobility and higher visible light response, as shown by chronoamperometry tests and diffuse reflectance spectroscopy.

MATERIALS CHEMISTRY AND PHYSICS 256, 123651, 2020. DOI: 10.1016/j.matchemphys.2020.123651

[P415-2020] "y Role of sphingomyelin on the interaction of the anticancer drug gemcitabine hydrochloride with cell membrane models"

Materon, E. M.; Nascimento, G. F.; **Shimizu, F. M.*;** Camara, A. S.; Sandrino, B.; Faria, R. C.; Oliveira Jr, O. N.

The fight against drug resistance in chemotherapy requires a molecular-level understanding of the drug interaction with cell membranes, which today is feasible with membrane models. In this study, we report on the interaction of gemcitabine (GEM), a pyrimidine nucleoside antimetabolite used to treat pancreatic cancer, with Langmuir films that mimic healthy and cancerous cell membranes. The cell membrane models were made with eight compositions of a quaternary mixture containing 1,2-dipalmitoyl-sn-glycerol-3-phosphocholine (DPPC), 1,2-dipalmitoyl-sn-glycero-3-phosphoserine (DPPS), sphingomyelin (SM), and cholesterol (CHOL). The relative concentration of SM was increased so that four of these compositions represented cancerous cells. GEM was found to increase the mean molecular area, also increasing their surface elasticity, with stronger interactions being observed for membranes corresponding to cancerous cells.

More specifically, GEM penetrated deepest in the membrane with the highest SM concentration (40 mol%), as inferred from polarization-modulated infrared reflection absorption spectroscopy (PM-IRRAS). This finding was confirmed with molecular dynamics simulations that also indicated how GEM approaches the membrane, which could be useful for guiding the design of drug delivery systems. The experimental and simulation results are consistent with the preferential attachment of GEM onto cancerous cells and highlight the role of SM on drug-cell interactions.

COLLOIDS AND SURFACES B-BIOINTERFACES 196, 111357, 2020. DOI: 10.1016/j.colsurfb.2020.111357

Eventos publicados 2020

[P416-2020] "NON-INVASIVE OPTICAL CBF MONITORING DURING MECHANICAL THROMBECTOMY"

Favilla, C.; **Forti, R.*;** Cummings, S.; Baker, W.; Detre, J.; Kasner, S.; Mullen, M.; Kung, D.; Kofke, W.; Balu, R.; **Mesquita, R.*;** Yodh, A.

INTERNATIONAL JOURNAL OF STROKE 15[1_SUPPL][SI], 604-604, 2020. DOI: 10.1177/1747493020963387

World Stroke Congress Abstracts, 2020

Correções 2020

[Co003-2020] "Search for photons with energies above 10(18) eV using the hybrid detector of the Pierre Auger Observatory (vol 04, 009, 2017)"

Aab, A.; Abreu, P. Aglietta, M.; **Chinellato, J. A.*; Franco, D. D.*; Castro, M. L. D.*; Dobrigkeit, C.*; Fauth, A. C.*; Payeras, A. M.*; Muller, M. A.***; et al. Pierre Auger Collaboration

JOURNAL OF COSMOLOGY AND ASTROPARTICLE PHYSICS [9], E02, 2020. DOI: 10.1088/1475-7516/2020/09/E02

***Autores da comunidade IFGW**
Fonte: Web of Science on-line (WOS)

Artigos publicados 2021

[P001-2021] "A DFT investigation of the electronic, optical, and thermoelectric properties of pentadiamond"

Tromer, R. M.*; Felix, L. C.*; Woellner, C. F.; Galvao, D. S.*

Recently, a new 3D carbon allotrope named pentadiamond was proposed composed by mixed sp 2 and sp 3 like hybridization. In this work, we have carried out a detailed investigation of the electronic, optical and thermoelectric properties of pentadiamond structure using first-principles methods. Our results show that pentadiamond has an indirect bandgap semiconductor of 2.50 eV with GGA-PBE and 3.31 eV with HSE06. Its static dielectric constant is 4.70 and the static refractive index is 2.16. Pentadiamond presents low reflectivity, making it a good structure to be used as a UV collector. Also, pentadiamond is a material that presents good thermoelectric properties.

CHEMICAL PHYSICS LETTERS 763, 138210, 2021. DOI: 10.1016/j.cplett.2020.138210

[P002-2021] "A novel self-aligned double patterning integrated with Ga+ focused ion beam milling for silicon nanowire definition"

Rosa, A. M.; Leonhardt, A.; Souza, L. O. de; Lima, L. P. B.; **Santos, M. V. P. dos***; Manera, L. T.; Diniz, J. A.

Self-aligned double (SADP) or quadruple (SAQP) patternings have been used to obtain sub-resolution lithographies (sub-10 nm). For this purpose, usually, these patternings are integrated with 193 nm immersion (193iL), extreme ultra-violet (EUVL) and electron beam (EBL) lithographies. In this work, SADPs are integrated with Ga+ Focused Ion Beam (FIB) milling, which is a novel alternative to traditional 193iL, EUVL and EBL, mainly for prototyping of nanodevices. Furthermore, the FIB milling is a maskless process, thus being more flexible than EBL and cheaper than EUVL. The FIB milling was carried out on the a-Si:H/Al (deposited on Si substrate) to pattern the parallel Al nanowires (AlNWs), which are used as mandrel in our SADP. The a-Si:H layer, used as spacer in our SADP, also is an effective barrier against the Ga+ ion bombardment directly on Al surface, avoiding damages on the AlNW mandrel. Thus, after FIB milling, SADP and plasma etch steps, Silicon Nano-Wires (SiNWs), with dimensions (extracted by Scaning Electron Microscopy (SEM)) of fin width and pitch of 35 nm and 170 nm, respectively, were obtained. This is an excellent result, similar to obtained by SADP methods integrated with traditional lithographies. Therefore, our SADP with FIB milling is a flexible alternative to obtain SiNWs for 3D nanostructure technologies prototypes. Furthermore, a last important result, extracted from energy dispersive x-ray spectroscopy (EDS) spectrum, is the Ga peak absence, indicating that no trace of gallium (for an EDS detection limit of 1%) could be detected into SiNWs. This result agrees the TRIM (Transport and Range of Ions in Matter) simulation of gallium ion implantation in a-Si:H/Al structure.

MICROELECTRONIC ENGINEERING 237, 111493, 2021. DOI: 10.1016/j.mee.2020.111493

[P003-2021] "Computational study of elastic, structural stability and dynamics properties of penta-graphene membrane"

De Sousa, J. M.; Aguiar, A. L.; Girao, E. C.; **Fonseca, A. F.***; Souza, A. G.; **Galvao, D. S.***

Recently, a new two-dimensional carbon allotrope called Penta--graphene membrane was proposed. The Pentagraphene membrane exhibits interesting mechanical and electronic properties, including typical band gap values of semiconducting materials.

Penta-graphene has a Cairo-tiling-like 2D lattice of non co-planar pentagons and its mechanical properties still have not been fully investigated. In this work, we combined reactive molecular dynamics (MD) simulations and density functional theory (DFT) calculations to investigate the mechanical properties and fracture patterns of Penta-graphene membranes under tensile stress. We show that Penta-graphene membranes can hold up to 20% of strain and that fracture occurs only after substantial dynamical bond breaking and the formation of 7, 8 and 11 carbon rings, as well as carbon chains. The stress-strain behavior was observed to follow two regimes, one exhibiting linear elasticity followed by a plastic one, involving carbon atom re-hybridization with the formation of carbon rings and chains.

CHEMICAL PHYSICS 542, 111052, 2021. DOI: 10.1016/j.chemphys.2020.111052

[P004-2021] "Correlations of azimuthal anisotropy Fourier harmonics with subevent cumulants in pPb collisions at root s(NN)=8.16 TeV"

Sirunyan, A. M.; Tumasyan, A.; **Chinellato, J. A.*; Tonelli Manganote, E. J.***; et al.
CMS Collaboration

Event-by-event long-range correlations of azimuthal anisotropy Fourier coefficients (v(n)) in 8.16 TeV pPb data, collected by the CMS experiment at the CERN Large Hadron Collider, are extracted using a subevent four-particle cumulant technique applied to very low multiplicity events. Each combination of four charged particles is selected from either two, three, or four distinct subevent regions of a pseudorapidity range from -2.4 to 2.4 of the CMS tracker, and with transverse momentum between 0.3 and 3.0 GeV. Using the subevent cumulant technique, correlations between v(n) of different orders are measured as functions of particle multiplicity and compared to the standard cumulant method without subevents over a wide event multiplicity range. At high multiplicities, the v(2) and v(3) coefficients exhibit an anticorrelation; this behavior is observed consistently using various methods. The v(2) and v(4) correlation strength is found to depend on the number of subevents used in the calculation. As the event multiplicity decreases, the results from different subevent methods diverge because of different contributions of noncollective or few-particle correlations. Correlations extracted with the four-subevent method exhibit a tendency to diminish monotonically toward the lowest multiplicity region (about 20 charged tracks) investigated. These findings extend previous studies to a significantly lower event multiplicity range and establish the evidence for the onset of long-range collective multiparticle correlations in small system collisions.

PHYSICAL REVIEW C 103[1], 014902, 2021. DOI: 10.1103/PhysRevC.103.014902

[P005-2021] "Dark Energy Survey year 3 results: point spread function modelling"

Jarvis, M.; Bernstein, G. M.; Amon, A.; **Navarro-Alsina, A.*;** et al. DES Collaboration

We introduce a new software package for modelling the point spread function (PSF) of astronomical images, called PIFF (PSFs In the Full FOV), which we apply to the first three years (known as Y3) of the Dark Energy Survey (DES) data. We describe the relevant details about the algorithms used by PIFF to model the PSF, including how the PSF model varies across the field of view (FOV). Diagnostic results show that the systematic errors from the PSF modelling are very small over the range of scales that are important for the DES Y3 weak lensing analysis. In particular, the systematic errors from the PSF modelling are significantly smaller than the corresponding results from the DES year one (Y1) analysis. We also briefly describe some planned improvements to PIFF that we expect to further reduce the modelling errors in future analyses.

MONTHLY NOTICES OF THE ROYAL ASTRONOMICAL SOCIETY 501[1], 1282-1299, 2021. DOI: 10.1093/mnras/staa3679

[P006-2021] "Designing of strongly confined short-wave Brillouin phonons in silicon waveguide periodic lattices"

Zurita, R. O.*; Wiederhecker, G. S.*; Alegre, T. P. M.*

We propose a feasible waveguide design optimized for harnessing Stimulated Brillouin Scattering with long-lived phonons. The design consists of a fully suspended ridge waveguide surrounded by a 1D phononic crystal that mitigates losses to the substrate while providing the needed homogeneity for the build-up of the optomechanical interaction. The coupling factor of these structures was calculated to be G(B)/Q(m) = 0.54 (W m)(-1) for intramodal backward Brillouin scattering with its fundamental TE-like mode and G(B)/Q(m) =4.5 (W m)(-1) for intramodal forward Brillouin scattering. The addition of the phononic crystal provides a 30 dB attenuation of the mechanical displacement after only five unitary cells, possibly leading to a regime where the acoustic losses are only limited by fabrication. As a result, the total Brillouin gain, which is proportional to the product of the coupling and acoustic quality factors, is nominally equal to the idealized fully suspended waveguide.

OPTICS EXPRESS 29[2], 1736-1748, 2021. DOI: 10.1364/OE.413770

[P007-2021] "Discovery of a candidate binary supermassive black hole in a periodic quasar from circumbinary accretion variability"

Liao, W. T.; Chen, Y. C.; **Sobreira, F.*;** et al. DES Collaboration

Binary supermassive black holes (BSBHs) are expected to be a generic byproduct from hierarchical galaxy formation. The final coalescence of BSBHs is thought to be the loudest gravitational wave (GW) siren, yet no confirmed BSBH is known in the GW-dominated regime. While periodic quasars have been proposed as BSBH candidates, the physical origin of the periodicity has been largely uncertain. Here, we report discovery of a periodicity (p = 1607 +/- 7 d) at 99.95 per cent significance (with a global p value of similar to 10(-3) accounting for the look elsewhere effect) in the optical light curves of a redshift 1.53 quasar, SDSS J025214.67-002813.7. Combining archival Sloan Digital Sky Survey data with new, sensitive imaging from the Dark Energy Survey, the total similar to 20-yr time baseline spans similar to 4.6 cycles of the observed 4.4-yr (rest frame 1.7-yr) periodicity. The light curves are best fit by a bursty model predicted by hydrodynamic simulations of circumbinary accretion discs. The periodicity is likely caused by accretion rate modulation by a milli-parsec BSBH emitting GWs, dynamically coupled to the circumbinary accretion disc. A bursty hydrodynamic variability model is statistically preferred over a smooth, sinusoidal model expected from relativistic Doppler boost, a kinematic effect proposed for PG1302-102. Furthermore, the frequency dependence of the variability amplitudes disfavours Doppler boost, lending independent support to the circumbinary accretion variability hypothesis. Given our detection rate of one BSBH candidate from circumbinary accretion variability out of 625 quasars, it suggests that future large, sensitive synoptic surveys such as the Vera C. Rubin Observatory Legacy Survey of Space and Time may be able to detect hundreds to thousands of candidate BSBHs from circumbinary accretion with direct implications for Laser Interferometer Space Antenna.

MONTHLY NOTICES OF THE ROYAL ASTRONOMICAL SOCIETY 500[3], 4025-4041, 2021. DOI: 10.1093/mnras/staa3055

[P008-2021] "Distributed Pressure Sensing Using an Embedded-Core Capillary Fiber and Optical Frequency Domain Reflectometry"

Gerosa, R. M.; **Osorio, J. H.***; Lopez-Cortes, D.; **Cordeiro, C. M. B.***; Matos, C. J. S. de

In this paper, we describe a distributed pressure sensor using a simplified and high sensitivemicrostructured optical fiber - the embedded-core fiber - and autocorrelation analysis of the data obtained from an optical frequency domain reflectometer (OFDR). The special fiber consists of a microcapillary, which has a germanium-doped core placed within the capillary wall. When this structure is subjected to pressure variations, an asymmetric stress distribution is induced within the fiber, entailing birefringence variations. Here, we show that the use of a commercial OFDR with submillimeter resolutiontogether with an autocorrelationdata analysis routine in the spectral domain allows mapping the fiber birefringence and performing distributed pressure sensing. In the experiments, the fiber passed through two pressure chambers, which allowed for pressure to be locally and independently applied. No cross-sensitivity between the pressure points was observed. The embedded-core fiber exhibited a birefringence sensitivity to pressure of 3.8x10(-7) bar(-1), which is 21% higher than thatmeasured in commercial photonic crystal fibers using the same setup.

IEEE SENSORS JOURNAL 21, 1, 360-365, 2021. DOI: 10.1109/JSEN.2020.3013983

[P009-2021] "Epitaxial growth, electronic hybridization and stability under oxidation of monolayer MoS2 on Ag(111)"

Amaral, G. M. do*; Tonon, I. da C.*; Roman, R. J. P.*; Plath, H. de O.*; Taniguchi, T. M.*; Lima, L. H. de; **Zagonel, L. F.*; Landers, R.*; Siervo, A. de***

The plethora of new transition metal dichalcogenides (TMDs) materials have attracted a major attention during the last years due to a diversity of new possibilities of applications in different areas from electronic and photonic devices to new sensors and catalysts, as well as a large playground of 2D materials to explore new physical phenomena. Many efforts have been done to develop new growth techniques that can produce single-layer TMDs in large areas and with high quality (low density of defects). Another important issue for electronic device integration is how to perform electrical contacts that show a metallic behavior instead semiconductor junctions. In this work, we have systematically studied the epitaxial growth of MoS2 on Ag(111) using the physical vapor deposition method (PVD). The results, based on a multiple technique approach, demonstrate that is possible to produce a single-layer 1H -MoS2 film on Ag(111). The material presents a metallic behavior due to an electronic hybridization between the MoS2 states and the Ag(111) states as results of the strong TMD-substrate interaction at the interface. This metallic character is preserved even after exposure to atmosphere and hostile oxidation environment which indicates that silver is probably an excellent candidate to perform metal contacts on sulfur-based TMDs.

APPLIED SURFACE SCIENCE 538, 148138, 2021. DOI: 10.1016/j.apsusc.2020.148138

[P010-2021] "Evidence for electroweak production of four charged leptons and two jets in proton-proton collisions at root s=13 TeV"

Sirunyan, A. M.; Tumasyan, A.; Adam, W.; **Chinellato, J. A.*; Tonelli Manganote, E. J.***; et al. CMS Collaboration

Evidence is presented for the electroweak (EW) production of two jets (jj) in association with two Z-bosons and constraints on anomalous quartic gauge couplings are set. The analysis is based on a data sample of proton-proton collisions at root s = 13 TeVcollected with the CMS detector in 2016-2018, and corresponding to an integrated luminosity of 137 fb(-1). The search is performed in the fully leptonic final state ZZ -> lll'l', where l, l' = e, mu. The EW production of two jets in association with two Zbosons is measured with an observed (expected) significance of 4.0 (3.5) standard deviations. The cross sections for the EW production are measured in three fiducial volumes and the result is sigma(EW)(pp -> ZZjj -> lll'l'jj) = 0.33(-0.10)(+0.11)(stat)(-0.03)(+0.04)(syst) fbin the most inclusive volume, in agreement with the standard model prediction of 0.275 +/- 0.021fb. Measurements of total cross sections for jj production in association with two Zbosons are also reported. Limits on anomalous quartic gauge couplings are derived in terms of the effective field theory operators T0, T1, T2, T8, and T9.

PHYSICS LETTERS B 812, 135992, 2021. DOI: 10.1016/j.physletb.2020.135992

[P011-2021] "Graphene-based nanoscale version of da Vinci's reciprocal structures"

Fonseca, A. F.*; Galvao, D. S.*

A reciprocal structure (RS) is a mechanical resistant structure formed by a set of self-supporting elements satisfying certain conditions of structural reciprocity (SR). The first condition is that each element of the structure has to support and be supported by the others. The second condition is that these functions cannot occur in the same part of the element. These two properties make beams and two-dimensional materials very much appropriate to build RSs. Commonly seen in floors or roofs, SR is also present in art, religious symbols, and decorative objects. Da Vinci has drawn several examples of such RSs. Here, thermal stability and mechanical resistance against impacts of simple nano versions of da Vinci's RSs based on graphene nanoribbons, were investigated through fully atomistic molecular dynamics (MD) simulations. We considered structures with three and four joins with and without RS topologies. Our MD results showed that 3-fold RSs are not thermally stable and that the 4-fold RSs can become thermally stable as long as the graphene nanoribbons have their external extremities fixed and either are not lengthy or have a kind of notch at the nanoribbons junctions. For these thermally stable structures, our results show that those with RS topologies are more impact resistant than those without SR, despite the fact that the used graphene nanoribbons are highly pliable. We discuss these results in terms of the number of joins, energy absorption, and stress on the structures. We discuss possible applications in nanoengineering.

COMPUTATIONAL MATERIALS SCIENCE 187, 110105, 2021. DOI: 10.1016/j.commatsci.2020.110105

[P012-2021] "High-frequency GaAs optomechanical bullseye resonator"

Carvalho, N. C.*; Benevides, R.*; Menard, M.; **Wiederhecker, G. S.*; Frateschi, N. C.*; Alegre, T. P. M.***

The integration of optomechanics and optoelectronics in a single device opens new possibilities for developing information technologies and exploring fundamental phenomena. Gallium arsenide (GaAs) is a well-known material that can bridge the gap between the functionalities of optomechanical devices and optical gain media.

Here, we experimentally demonstrate a high-frequency GaAs optomechanical resonator with a ring-type bullseye geometry that is unprecedented in this platform. We measured mechanical modes up to 3.4 GHz with quality factors of 4000 (at 80 K) and optomechanical coupling rates up to 39 kHz at telecom wavelengths. Moreover, we investigated the material symmetry break due to elastic anisotropy and its impact on the mechanical mode spectrum. Finally, we assessed the temperature dependence of the mechanical losses and demonstrated the efficiency and anisotropy resilience of the bullseye anchor loss suppression, indicating that lower temperature operation may allow mechanical quality factors over 10(4). Such characteristics are valuable for active optomechanics, coherent microwave to optics conversion via piezomechanics, and other implementations of high-frequency oscillators in III-V materials.

APL PHOTONICS 6[1], 016104, 2021. DOI: 10.1063/5.0024511

[P013-2021] "Hybrid magneto-luminescent iron oxide nanocubes functionalized with europium complexes: synthesis, hemolytic properties and protein corona formation"

Costa, L. S. da*; Khan, L. U.; Franqui, L. S.; Delite, F. D.; **Muraca, D.*;** Martinez, D. S. T.; **Knobel, M.***

The use of hybrid nanostructures based on magneto-luminescent properties is a promising strategy for nano-bio applications and theranostics platforms. In this work, we carried out the synthesis and functionalization of iron oxide nanocubes (IONCs) to obtain multifunctional hybrid nanostructures towards biomedical applications. The IONCs were functionalized with tetraethylorthosilicate, thenoyltrifluoroacetone-propyktriethoxysilane and europium(III)-dibenzoyErnethane complexes to obtain the materiaLs termed as IOCNCs@SiO2, IONCs@SiO(2)TTA, IONCs@SiO(2) TTA-Eu and IONCs@SiO2-TTA-Eu-DBM, respectively. Then, the biological interactions of these nanostructures with red blood cells - RBCs (hemolysis) and human blood plasma (protein corona formation) were evaluated. The XPS spectrocopy and EDS chemical mapping analysis showed that each domain is homogeneously occupied in the hybrid material, with the magnetic core at the center and the Luminescent domain on the surface of the hybrid nanomaterial with a core@shell Like structure. Futhermore, after each functionalization step, the nanomaterial surface charge drastically changed, with critical impact on RBC lysis and corona formation. While IONCs@SiO2 and IONCs@ SiO2-TTA-Eu-DBM showed hemolytic properties in a dose-dependent manner, the IONCs@SiO(2)TTA-Eu did not present any hemolytic effect up to 300 mu g mL(.)(-1) Protein corona results showed a pattern of selective adsorption of proteins with each surface of the synthesized hybrid materials. However, as a general result, a suppression of hemolysis after protein corona formation in all tests was verified. Finally, this study provides a solid background for further applications of these hybrid magneto-luminescent materials containing new surface functionalities in the emerging field of medical nanobiotechnology.

JOURNAL OF MATERIALS CHEMISTRY B 9[2], 428-439, 2021. DOI: 10.1039/d0tb02454f

[P014-2021] "Improvements on perturbative oscillation formulas including non-standard neutrino interactions"

Chaves, M. E.*; Gratieri, D. R.*; Peres, O. L. G.*

We use perturbation theory to obtain neutrino oscillation probabilities, including the standard mass-mixing paradigm and non-standard neutrino interactions (NSI). The perturbation is made on the standard parameters Delta m212/Delta m312<i and sin(2)(theta(13)) and on the non-diagonal NSI parameters, but keeps diagonal NSI parameters non-perturbated. We perform the calculation for the channels nu(mu) -> nu(e) and nu(mu) -> nu(mu). The resulting oscillation formulas are compact and present functional structure similar to the standard oscillation (SO) case. They apply to a wide range in the allowed NSI space of parameters and include the previous results from perturbative approaches as limit cases. Also, we use the compact formulas we found to explain the origin of the degeneracies in the neutrino probabilities in terms of the invariance of amplitude and phase of oscillations. Then we determine analytically the multiple sets of combinations of SO and NSI parameters that result in oscillation probabilities identical to the SO case.

JOURNAL OF PHYSICS G-NUCLEAR AND PARTICLE PHYSICS 48, 1, 015001, 2021. DOI: 10.1088/1361-6471/abae17

[P015-2021] "Influence of water on electrical and mechanical properties of self-assembled and self-healing PEM films"

Gaal, G.*; Jimenez, M. J. M.*; Alvarez, F.*; Rodrigues, V.*; Riul Jr., A.*

Self-healing coatings as thin films have been widely exploited in the last decade due to the conformational ability to adhere practically at any surface, bringing multiple regenerations in damaged areas. Poly(ethylene imine) (PEI) and poly(acrylic acid) (PAA) are the most used polyelectrolytes to grow self-healing layer-by-layer films; however, few studies have been dedicated to evaluate the role of water on the electrical and mechanical properties of the films. Multilayered (PEI/PAA) structures were easily self-assembled on various substrates, allowing homogeneous and semi-transparent coverages. We associate the exponential and linear growth regimes of (PEI/PAA) with changes in the electrical characteristics acquired after each step of the film formation. We demonstrated the central role of trapped water on the space charge accumulation at polymer/electrode interface, due to the presence of negative differential resistance regions, and the transition of the charge transport to a space charge regime after a critical potential. We have also investigated changes in the mechanical properties, showing the influence of trapped water in the film elastic modulus, wear resistance, and resistance to plastic deformation.

PROGRESS IN ORGANIC COATINGS 150, 105980, 2021. DOI: 10.1016/j.porgcoat.2020.105980

[P016-2021] "Intermediate type-I superconductors in the mesoscopic scale"

Cadorim, L. R.; Romaguera, A. R. de C.; Oliveira, I. G. de; Gomes, R. R.; **Doria, M. M.*;** Sardella, E.

M. Tinkham [Introduction to Superconductivity, 2nd ed. (Dover, Mineola, NY, 2004), Chap. 4, pp. 135-138] and P. G. de Gennes [Superconductivity of Metals andAlloys (Benjamin, New York, 1966), Chap. 6, pp. 199-201] described the existence of an intermediate type-I superconductor as a consequence of an external surface that affects the well-known classification of superconductors into type I and II. Here we consider the mesoscopic superconductor where the volume-to-area ratio is small and the effects of the external surface are enhanced. By means of the standard Ginzburg-Landau theory, the Tinkham-de Gennes scenario is extended to the mesoscopic type-I superconductor. We find additional features of the transition at the passage from the genuine to the intermediate type I. The latter has two distinct transitions, namely from a paramagnetic to diamagnetic response in descending field, and a quasi-type-II behavior as the critical coupling 1/root 2 is approached in ascending field. The intermediate type-I phase proposed here, and its corresponding transitions, reflect intrinsic features of the superconductor and not its geometrical properties.

PHYSICAL REVIEW B 103, 1, 014504, 2021. DOI: 10.1103/PhysRevB.103.014504

[P017-2021] " Investigating charge carrier scattering processes in anisotropic semiconductors through first-principles calculations: the case of p-type SnSe"

Chaves, A. S.*; Gonzalez-Romero, R. L.; Melendez, J. J.; **Antonelli, A.***

Efficient ab initio computational methods for the calculation of the thermoelectric transport properties of materials are of great interest for energy harvesting technologies. The constant relaxation time approximation (CRTA) has been largely used to efficiently calculate thermoelectric coefficients. However, CRTA usually does not hold for real materials. Here we go beyond the CRTA by incorporating realistic k-dependent relaxation time models of the temperature dependence of the main scattering processes, namely, screened polar and nonpolar scattering by optical phonons, scattering by acoustic phonons, and scattering by ionized impurities with screening. Our relaxation time models are based on a smooth Fourier interpolation of Kohn-Sham eigenvalues and its derivatives, taking into account non-parabolicity (beyond the parabolic or Kane models), degeneracy and multiplicity of the energy bands on the same footing, within very low computational cost. In order to test our methodology, we calculated the anisotropic thermoelectric transport properties of the low temperature phase (Pnma) of intrinsic p-type and hole-doped tin selenide (SnSe). Our results are in quantitative agreement with experimental data, regarding the evolution of the anisotropic thermoelectric coefficients with both temperature and chemical potential. Hence, from this picture, we also obtained the evolution and understanding of the main scattering processes of the overall thermoelectric transport in p-type SnSe.

PHYSICAL CHEMISTRY CHEMICAL PHYSICS 23[2], 900-913, 2021. DOI: 10.1039/d0cp05022a

[P018-2021] "Knee radiosynovectomy with Sm-153-hydroxyapatite compared to Y-90-hydroxyapatite: initial results of a prospective trial"

Santos, A. O.; Ricciardi, J. B. S.; Pagnano, R.; Pereira, L. F. M.; Sakuma, E. T.; Matsuda, M. M. N.; Bernardes, E. S.; Araujo, E. B.; Brunetto, S. Q.; **Takahashi, M. E. S.***; Brunetto, E. M.; Zulli, R.; Ozelo, M. C.; Etchebehere, E. C. S. C.

Introduction Radiosynovectomy (RS) with Y-90-hydroxyapatite (Y-90-HyA) aims to control knee hemarthrosis in hemophiliac patients to prevent secondary arthropathy. However, knee RS using Sm-153-hydroxyapatite (Sm-153-HyA) is considered less suitable due to the lower average soft tissue range and energy of Sm-153 for large joints, such as the knees. Purpose The objective of this investigation was to assess the efficacy and safety of knee RS with Sm-153-HyA, compared to Y-90-HyA. Methods Forty patients were prospectively assigned to undergo knee RS with Sm-153-HyA (n = 19) or with Y-90-HyA (n = 21). The frequency of hemarthrosis episodes before and after treatment were compared. Results After six months of knee RS, Sm-153-HyA and Y-90-HyA promoted a similar reduction of hemarthrosis episodes (50% and 66.7%, respectively). However, after 12 months of knee RS, the reduction of hemarthrosis episodes was significantly (p = 0.037) higher using Sm-153-HyA (87.5%) compared to Y-90-HyA (50.0%). This discrepancy was more pronounced (p = 0.002) for Sm-153-HyA compared to Y-90-HyA in adults/adolescents. Conclusion Knee radiosynovectomy with Sm-153-HyA is safe, reduces hemarthrosis episodes after 12 months of treatments, especially in adults/adolescents and even with grades III/IV arthropathy, similar to Y-90-HyA. Y-90-HyA seems to promote better hemarthrosis control in small children.

ANNALS OF NUCLEAR MEDICINE, Primeira data de acesso: Jan. 2021. DOI: 10.1007/s12149-020-01557-5

[P019-2021] "Measurement of Multiphase Flow by Tilted Optical Fiber Bragg Grating Sensor"

Aristilde, S.*; Soares, M. C. P.**; Cabral, T. D.*; Rodrigues, G.*;** Fujiwara, E.; Fruett, F.; Cordeiro, C. M. B.

Measuring multiphase flows is essential in the oil and gas industry and medicine, as well as to microfluidic-based analyses. This article presents an optical fiber sensor for assessing the speed of two-phase flows based on tilted fiber Bragg grating (TFBG). As the di*spersed slugs pass by the grating, resonance dips of cladding modes shift and work like a notch filter for a given wavelength; therefore, the TBFG can be interrogated in real-time according to an intensity-based, single-wavelength setup. The system is validated for samples comprised of water, oil, and air, yielding maximum relative error of 4.4% for speed measurements, whereas the sensor response can be tailored for different fluids by choosing the wavelength of the input light.

IEEE SENSORS JOURNAL 21, 2, 1534-1539, 2021. DOI: 10.1109/JSEN.2020.3016616

[P020-2021] "Measurements of production cross sections of polarized same-sign W boson pairs in association with two jets in proton-proton collisions at root s=13 TeV"

Sirunyan, A. M.; Tumasyan, A.; Adam, W.; **Chinellato, J. A.*; Tonelli Manganote, E. J.***; et al. CMS Collaboration

The first measurements of production cross sections of polarized same-sign (WW +/-)-W-+/- boson pairs in proton-proton collisions are reported. The measurements are based on a data sample collected with the CMS detector at the LHC at a center--of-mass energy of 13 TeV, corresponding to an integrated luminosity of 137 fb(-1). Events are selected by requiring exactly two same-sign leptons, electrons or muons, moderate missing transverse momentum, and two jets with a large rapidity separation and a large dijet mass to enhance the contribution of same-sign (WW +/-)-W-+/- scattering events. An observed (expected) 95% confidence level upper limit of 1.17 (0.88) fbis set on the production cross section for longitudinally polarized same-sign W-+/- W-+/- boson pairs. The electroweak production of same-sign W-+/- W-+/- boson pairs with at least one of the W bosons longitudinally polarized is measured with an observed (expected) significance of 2.3 (3.1) standard deviations.

PHYSICS LETTERS B 812, 136018, 2021. DOI: 10.1016/j.physletb.2020.136018

[P021-2021] "Metalation of 2HTCNPP on Ag(111) with Zn: Evidence for the Sitting atop Complex at Room Temperature"

Kuliga, J.; **Ferreirra, R. C. de. C.***; Adhikari, R.; Massicot, S.; Lepper, M.; Holzel, H.; Jux, N.; Marbach, H.; **Siervo, A. de***; Steinruck, H. P.

We study the interaction and metalation reaction of a free base 5,10,15,20-terakis(4-cyanophenyl)porphyrin (2HTCNPP) with post-deposited Zn atoms and the targeted reaction product Zn-5,10,15,20-terakis(4-cyanophenyl)porphyrin (ZnTCNPP) on a Ag(111) surface. The investigations are performed with scanning tunneling microscopy at room temperature after Zn deposition and subsequent heating. The goal is to obtain further insights in the metalation reaction and the influence of the cyanogroups on this reaction. The interaction of 2HTCNPP with post-deposited Zn leads to the formation of three different 2D ordered island types that coexist on the surface. All contain a new species with a bright appearance, which increases with the amount of post-deposited Zn. We attribute this to metastable SAT ("sitting atop") complexes formed by Zn and the macrocycle, that is, an intermediate in the metalation reaction to ZnTCNPP, which occurs upon heating to 500 K.

Interestingly, the activation barrier for the successive reaction of the SAT complex to the metalated ZnTCNPP species can also be overcome by a voltage pulse applied to the STM tip.

CHEMPHYSCHEM, Primeira data de acesso: Jan. 2021, DOI: 10.1002/cphc.202000883

[P022-2021] "Modeling Mito-nuclear Compatibility and Its Role in Species Identification"

Princepe, D.*; Aguiar, M. A. M. de*

Mitochondrial genetic material (mtDNA) is widely used for phylogenetic reconstruction and as a barcode for species identification. The utility of mtDNA in these contexts derives from its particular molecular properties, including its high evolutionary rate, uniparental inheritance, and small size. ButmtDNA may also play a fundamental role in speciation-as suggested by recent observations of coevolution with the nuclear DNA, along with the fact that respiration depends on coordination of genes from both sources. Here, we study how mito-nuclear interactions affect the accuracy of species identification by mtDNA, as well as the speciation process itself. We simulate the evolution of a population of individuals who carry a recombining nuclear genome and a mitochondrial genome inherited maternally. We compare a null model fitness landscape that lacks any mito--nuclear interaction against a scenario in which interactions influence fitness. Fitness is assigned to individuals according to their mito-nuclear compatibility, which drives the coevolution of the nuclear and mitochondrial genomes. Depending on the model parameters, the population breaks into distinct species and the model output then allows us to analyze the accuracy of mtDNA barcode for species identification. Remarkably, we find that species identification by mtDNA is equally accurate in the presence or absence of mito-nuclear coupling and that the success of the DNA barcode derives mainly from population geographical isolation during speciation. Nevertheless, selection imposed by mito-nuclear compatibility influences the diversification process and leaves signatures in the genetic content and spatial distribution of the populations, in three ways. First, speciation is delayed and the resulting phylogenetic trees are more balanced. Second, clades in the resulting phylogenetic tree correlate more strongly with the spatial distribution of species and clusters of more similar mtDNA's. Third, there is a substantial increase in the intraspecies mtDNA similarity, decreasing the number of alleles substitutions per locus and promoting the conservation of genetic information. We compare the evolutionary patterns observed in our model to empirical data from copepods (Tigriopus californicus). We find good qualitative agreement in the geographic patterns and the topology of the phylogenetic tree, provided the model includes selection based on mito-nuclear interactions. These results highlight the role of mito-nuclear compatibility in the speciation process and its reconstruction from genetic data.

SYSTEMATIC BIOLOGY 70[1], 133-144, 2021. DOI: 10.1093/sysbio/syaa044

[P023-2021] "Momentum-dependent flow fluctuations as a hydrodynamic response to initial geometry"

Hippert, M.*; Chinellato, D. D.*; Luzum, M.; Noronha, J.; Silva, T. N. da; **Takahashi, J.***

We propose a redefinition of the principal component analysis (PCA) of anisotropic flow that makes it more directly connected to fluctuations of the initial geometry of the system. Then, using state-of-the-art hydrodynamic simulations, we make an explicit connection between flow fluctuations and a cumulant expansion of the initial transverse geometry. In particular, we show that the second principal component of elliptic flow is generated by higher-order cumulants, and therefore probes smaller length scales of the initial state. With this information, it will be possible to put new constraints on properties of the early-time dynamics of a heavy-ion collision, including small-scale structure, as well as properties of the quark-gluon plasma.

NUCLEAR PHYSICS A 1005, SI, 121982, 2021. DOI: 10.1016/j.nuclphysa.2020.121982

[P024-2021] "Multidimensional coherent spectroscopy reveals triplet state coherences in cesium lead-halide perovskite nanocrystals"

Liu, A.; Almeida, D. B.; Bonato, L. G.; **Nagamine, G.*; Zagonel, L. F.***; Nogueira, A. F.; **Padilha, L. A.***; Cundiff, S. T.

Advances in optoelectronics require materials with novel and engineered characteristics. A class of materials that has garnered tremendous interest is metal-halide perovskites, stimulated by meteoric increases in photovoltaic efficiencies of perovskite solar cells. In addition, recent advances have applied perovskite nanocrystals (NCs) in light-emitting devices. It was found recently that, for cesium lead-halide perovskite NCs, their unusually efficient light emission may be due to a unique excitonic fine structure composed of three bright triplet states that minimally interact with a proximal dark singlet state. To study this fine structure without isolating single NCs, we use multidimensional coherent spectroscopy at cryogenic temperatures to reveal coherences involving triplet states of a CsPbI3 NC ensemble. Picosecond time scale dephasing times are measured for both triplet and inter-triplet coherences, from which we infer a unique exciton fine structure level ordering composed of a dark state energetically positioned within the bright triplet manifold.

SCIENCE ADVANCES 7[1], eabb3594, 2021. DOI: 10.1126/sciadv.abb3594

[P025-2021] "Negative entropy production rates in Drude--Sommerfeld metals"

Bonanca, M. V. S.*; Naze, P.*; Deffner, S.*

It is commonly accepted that in typical situations the rate of entropy production is non-negative. We show that this assertion is not entirely correct, not even in the linear regime, if a time-dependent, external perturbation is not compensated by a rapid enough decay of the response function. This is demonstrated for three variants of the Drude model to describe electrical conduction in noble metals, namely the classical free electron gas, the Drude-Sommerfeld model, and the extended Drude-Sommerfeld model. The analysis is concluded with a discussion of potential experimental verifications and ramifications of negative entropy production rates.

PHYSICAL REVIEW E 103[1], 012109, 2021. DOI: 10.1103/PhysRevE.103.012109

[P026-2021] "Nonequilibrium ensemble derivation of hydrodynamic heat transport and higher-order generalizations"

Rodrigues, C. G.; Silva, C. A. B.; **Ramos, J. G.*; Luzzi, R.***

Thermal transport in classical fluids is analyzed through higher-order generalized hydrodynamics (or mesoscopic hydrothermodynamics) depending on the evolution of the energy density and its fluxes of all orders. It is derived by a kinetic theory based on the nonequilibrium statistical ensemble formalism. A general system of coupled evolution equations is derived. Maxwell times, which are of significance to determine the character of the motion, are derived.

They also have an important role in the choice of the contraction of description (limitation in the number of fluxes to be retained) in the studies on hydrodynamic motions. In a description of order 1, an analysis of the technological process of thermal prototyping is presented.

INDIAN JOURNAL OF PHYSICS, Primeira data de acesso: JAN 2021. DOI: 10.1007/s12648-020-01968-0

[P027-2021] "Outlining cell interaction and inflammatory cytokines on UV-photofunctionalized mixed-phase TiO2 thin film"

Pantaroto, H. N.; Almeida, A. B. de; Gomes, O. P.; Matos, A. O.; **Landers, R.***; Casarin, R. C. V.; Silva, J. H. D. da; Nociti Jr., F. H.; Barao, V. A. R.

Photofunctionalization mediated by ultraviolet (UV) light seems to be a promising approach to improve the physico-chemical characteristics and the biological response of titanium (Ti) dental implants. Seeing that photofunctionalization is able to remove carbon from the surface, besides to promote reactions on the titanium dioxide (TiO2) layer, coating the Ti with a stable TiO2 film could potentialize the UV effect. Thus, here we determined the impact of UV-photofunctionalized mixed-phase (anatase and rutile) TiO2 films on the physico-chemical properties of Ti substrate and cell biology. Mixed-phase TiO2 films were grown by radiofrequency magnetron sputtering on commercially pure titanium (cpTi) discs, and samples were divided as follow: cpTi (negative control), TiO2 (positive control), cpTi UV, TiO2 UV (experimental). Photofunctionalization was performed using UVA (360 nm - 40 W) and UVC (250 nm - 40 W) lamps for 48 h. Surfaces were analyzed in terms of morphology, topography, chemical composition, crystalline phase, wettability and surface free energy. Pre-osteoblastic cells (MC3T3E1) were used to assess cell morphology and adhesion, metabolism, mineralization potential and cytokine secretion (IFN-gamma, TNF-alpha, IL-4, IL-6 and IL-17). TiO2-coated surfaces exhibited granular surface morphology and greater roughness. Photofunctionalization increased wettability ($p < 0.05$) and surface free energy ($p < 0.001$) on both surface conditions. TiO2-treated groups featured normal cell morphology and spreading, and greater cellular metabolic activity at 2 and 4 days ($p < 0.05$), whereas UV-photofunctionalized surfaces enhanced cell metabolism, cell adhered area, and calcium deposition (day 14) ($p < 0.05$). In general, assessed proteins were found slightly affected by either UV or TiO2 treatments. Altogether, our findings suggest that UV-photofunctionalized TiO2 surface has the potential to improve pre-osteoblastic cell differentiation and the ability of cells to form mineral nodules by modifying Ti physico-chemical properties towards a more stable context. UV-modified surfaces modulate the secretion of key inflammatory markers.

MATERIALS SCIENCE & ENGINEERING C-MATERIALS FOR BIOLOGICAL APPLICATIONS 118, 111438, 2021. DOI: 10.1016/j.msec.2020.111438

[P028-2021] "Search for dark matter produced in association with a leptonically decaying Z boson in proton-proton collisions at root s=13TeV"

Sirunyan, A. M.; Tumasyan, A.; Adam, W.; **Chinellato, J. A.*; Tonelli Manganote, E. J.***; et al. CMS Collaboration

A search for dark matter particles is performed using events with a Z boson candidate and large missing transverse momentum. The analysis is based on proton-proton collision data at a center-of-mass energy of 13 TeV, collected by the CMS experiment at the LHC in 2016-2018, corresponding to an integrated luminosity of 137 fb(-1). The search uses the decay channels Z -> ee and Z -> mu mu. No significant excess of events is observed over the background expected from the standard model. Limits are set on dark matter particle production in the context of simplified models with vector, axial-vector, scalar, and pseudoscalar mediators, as well as on a two-Higgs--doublet model with an additional pseudoscalar mediator. In addition, limits are provided for spin-dependent and spin--independent scattering cross sections and are compared to those from direct-detection experiments. The results are also interpreted in the context ofmodels of invisible Higgs boson decays, unparticles, and large extra dimensions.

EUROPEAN PHYSICAL JOURNAL C 81[1], 13, 2021. DOI: 10.1140/epjc/s10052-020-08739-5

[P029-2021] "Search for top squark pair production using dilepton final states in pp collision data collected at root s=13TeV"

Sirunyan, A. M.; Tumasyan, A.; Adam, W.; **Chinellato, J. A.*; Tonelli Manganote, E. J.***; et al. CMS Collaboration

A search is presented for supersymmetric partners of the top quark (top squarks) in final states with two oppositely charged leptons (electrons or muons), jets identified as originating from bquarks, and missing transverse momentum. The search uses data from proton-proton collisions at root s = 13 TeV collected with the CMS detector, corresponding to an integrated luminosity of 137 fb(-1). Hypothetical signal events are efficiently separated from the dominant top quark pair production background with requirements on the significance of the missing transverse momentum and on transverse mass variables. No significant deviation is observed from the expected background. Exclusion limits are set in the context of simplified supersymmetric models with pair-produced lightest top squarks. For top squarks decaying exclusively to a top quark and a lightest neutralino, lower limits are placed at 95% confidence level on the masses of the top squark and the neutralino up to 925 and 450 GeV, respectively. If the decay proceeds via an intermediate chargino, the corresponding lower limits on the mass of the lightest top squark are set up to 850 GeV for neutralino masses below 420 GeV. For top squarks undergoing a cascade decay through charginos and sleptons, the mass limits reach up to 1.4 TeV and 900 GeV respectively for the top squark and the lightest neutralino.

EUROPEAN PHYSICAL JOURNAL C 81[1], 3, 2021. DOI: 10.1140/epjc/s10052-020-08701-5

[P030-2021] "Time-Rescaling of Dirac Dynamics: Shortcuts to Adiabaticity in Ion Traps and Weyl Semimetals"

Roychowdhury, A.; **Deffner, S.***

Only very recently, rescaling time has been recognized as a way to achieve adiabatic dynamics in fast processes. The advantage of time-rescaling over other shortcuts to adiabaticity is that it does not depend on the eigenspectrum and eigenstates of the Hamiltonian. However, time-rescaling requires that the original dynamics are adiabatic, and in the rescaled time frame, the Hamiltonian exhibits non-trivial time-dependence. In this work, we show how time-rescaling can be applied to Dirac dynamics, and we show that all time--dependence can be absorbed into the effective potentials through a judiciously chosen unitary transformation. This is demonstrated for two experimentally relevant scenarios, namely for ion traps and adiabatic creation of Weyl points.

ENTROPY 23[1], 81, 2021. DOI: 10.3390/e23010081

[P031-2021] "Use of amorphous Nb2O5 and Nb2O5/Al2O3 as acid catalysts for the dehydration of xylose to furfural"

Lima, L. F. de; Lima, J. L. M.; Jorqueira, D. S. S.; **Landers, R.***; Moya, S. F.; Suppino, R. S.

This work compared the catalytic performance of the amorphous Nb2O5 (NB) and 12 wt% Nb2O5/Al2O3 (NB-AL) catalysts for the xylose dehydration to furfural carried out for 6 h at 140 and 160 degrees C using water or a 1:0.8 (v/v) water/isopropanol mixture as solvents. The solids were characterized by XRD, N-2 adsorption, TGA, XPS, TPD-NH3 and FTIR-Pyridine. Results indicated a specific surface area of 144 and 108 m(2)/g and an average pore diameter of 44 and 76 angstrom to NB and NB-AL respectively. The solids presented similar density of acid sites (6.0 for NB and 5.7 mu molNH(3)/m(2) for NB-AL), but different strength distribution of the acid sites. Moreover, the fraction of Bronsted acid sites on NB was 27%, whereas on NB-AL it was only 2%. Concerning the catalytic tests, the highest conversion of xylose for NB and NB-AL (99.0 and 91.1%, respectively) was achieved for the reactions at 160 degrees C in water/isopropanol mixture, whilst the highest selectivities to furfural were obtained in reactions with water at 160 degrees C (60.1% to NB and 35.1% to NB-AL). Finally, using water as solvent, the selectivity to furfural increased with both catalysts at the highest temperature, though the carbon balance decreased.

REACTION KINETICS MECHANISMS AND CATALYSIS, Primeira data de acesso: JAN 2021. DOI: 10.1007/s11144-021-01931-y

Material Editorial 2021

[Ma001-2021] "When silicon is like a cuprate"

Miranda, E.*

Recent advances in spectroscopy give access to the decay time of excitations in disordered insulating silicon close to the metal-insulator transition, revealing similarities to high-temperature cuprate superconductors.

NATURE PHYSICS, Primeira data de acesso: JAN 2021. DOI: 10.1038/s41567-020-01162-3

Correções 2021

[Co001-2021] "Experimental Study on Glass and Polymers: Determining the Optimal Material for Potential Use in Terahertz Technology (vol 8, pg 97204, 2020)"

Islam, M. S.; **Cordeiro, C. M. B.***; Nine, M. J.; Sultana, J.; Cruz, A. L. S.; Dinovitser, A.; Ng, B. W. H.; Ebendorff-Heidepriem, H.; Losic, D.; Abbott, D.

Resumo: Fig. 4 in reference [1] is after [2].

IEEE ACCESS 9, 2705-2705, 2021. DOI: 10.1109/ACCESS.2020.3047311

[Co002-2021] "Is every strong lens model unhappy in its own way? Uniform modelling of a sample of 13 quadruply+ imaged quasars (vol 483, pg 5671, 2019)"

Shajib, A. J.; Birrer, S.; Treu, T.; **Sobreira, F.***; et al.

MONTHLY NOTICES OF THE ROYAL ASTRONOMICAL SOCIETY 501[2], 2833-2835, 2021 DOI: 10.1093/mnras/staa3562

***Autores da comunidade IFGW**
Fonte: Web of Science on-line (WOS)

Defesas de Dissertações do IFGW

[D001-2021] "Modelagem de nanoantenas ópticas como lançadores polaritônicos otimizados para dispositivos nanofotônicos"
Aluno: Rafael Alves Mayer
Orientador: Prof. Dr. Raul de Oliveira Freitas
Data: 26/02/2021

[D002-2021] "Correções de ótica linear e acoplamento aplicadas ao comissionamento do Sirius"
Aluno: Murilo Barbosa Alves
Orientador: Prof. Dr. Antonio Rubens Britto de Castro
Data: 05/03/2021

Defesas de Teses do IFGW

[T001-2021] "Fabricação e caracterização de filmes finos poliméricos com nanopartículas metálicas embebidas visando aplicação em sensores"
Aluno: Rafael Cintra Hensel Ferreira
Orientador: Prof. Dr. Varlei Rodrigues
Data: 26/01/2021

Fonte: Portal IFGW/Pós-graduação - Agenda de Colóquios, Defesas e Seminários.
Disponível em: http://portal.ifi.unicamp.br/pos-graduacao

***Observação:** Não ocorreram ainda este ano defesas de teses e dissertações, com orientadores ou banca do IFGW, referentes ao Programa de Pós-Graduação Multiunidades em Ensino de Ciências e Matemática – Mestrado e Doutorado (PECIM) da Unicamp.
Fonte: Página do PECIM - **Disponível em:** https://www.pecim.unicamp.br/bancas

Abstracta

Instituto de Física
Diretor: Prof. Dr. Pascoal José Giglio Pagliuso
Diretora Associada: Profa. Dra. Mônica Alonso Cotta
Universidade Estadual de Campinas - UNICAMP
Cidade Universitária Zeferino Vaz
13083-859 - Campinas - SP - Brasil
e-mail: secdir@ifi.unicamp.br
Fone: +55 19 3521-5300

Publicação

Biblioteca do Instituto de Física Gleb Wataghin
http://portal.ifi.unicamp.br/biblioteca

Diretora Técnica: Sandra Maria Carlos Cartaxo
Coordenadora da Comissão de Biblioteca: Profa. Dra. Arlene Cristina Aguilar

Elaboração:
Maria Graciele Trevisan (Bibliotecária)
Ayres Neri da Cunha Junior (Técnico Administrativo)
contato: infobif@ifi.unicamp.br